Inorganic Chemistry

Article

pubs.acs.org/IC

Synthesis, Magnetostructural Correlation, and Catalytic Promiscuity of Unsymmetric Dinuclear Copper(II) Complexes: Models for Catechol Oxidases and Hydrolases

Renata E. H. M. B. Osório,[†] Rosely A. Peralta,[†] Adailton J. Bortoluzzi,[†] Vicente R. de Almeida,[†] Bruno Szpoganicz,[‡] Franciele L. Fischer,[§] Hernán Terenzi,*[,§] Antonio S. Mangrich,[⊥] Karen Mary Mantovani,[⊥] Dalva E. C. Ferreira,[¶] Willian R. Rocha,[¶] Wolfgang Haase,[∥] Zbigniew Tomkowicz,[∥,▽] Ademir dos Anjos,[#] and Ademir Neves*[,†]

[†]Laboratório de Bioinorgânica e Crystalografia (LABINC), Departamento de Química, [‡]Laboratório de Equilíbrio Químico, Departamento de Química, and [§]Centro de Biologia Molecular Estrutural, Departamento de Bioquímica, Universidade Federal de Santa Catarina, 88040-900 Florianópolis, Santa Catarina, Brazil

[⊥]Departamento de Química, Universidade Federal do Paraná, 81531-970 Curitiba, Paraná, Brazil

[¶]Departamento de Química, Instituto de Ciências Exatas, Universidade Federal de Minas Gerais, Campus Universitário Pampulha, 31270-901 Pampulha, Belo Horizonte, Minas Gerais, Brazil

[∥]Institut für Physikalishe Chemie, Technische Universität Darmstadt, Petersenstraße 20, D-64287-Darmstadt, Germany

[▽]Institute of Physics, Reymonta 4, Jagiellonian University, PL-30-059 Krakow, Poland

[#]Universidade Estadual de Mato Grosso do Sul, 79950-000 Unidade Universitária de Naviraí, Mato Grosso do Sul, Brazil

Supporting Information

ABSTRACT: Herein, we report the synthesis and characterization, through elemental analysis, electronic spectroscopy, electrochemistry, potentiometric titration, electron paramagnetic resonance, and magnetochemistry, of two dinuclear copper(II) complexes, using the unsymmetrical ligands *N*′,*N*′,*N*-tris(2-pyridylmethyl)-*N*-(2-hydroxy-3,5-di-*tert*-butylbenzyl)-1,3-propanediamin-2-ol (**L1**) and *N*′,*N*′-bis(2-pyridylmethyl)-*N*,*N*-(2-hydroxybenzyl)(2-hydroxy-3,5-di-*tert*-butylbenzyl)-1,3-propanediamin-2-ol (**L2**). The structures of the complexes $[Cu_2(\mathbf{L1})(\mu\text{-OAc})](ClO_4)_2\cdot(CH_3)_2CHOH$ (**1**) and $[Cu_2(\mathbf{L2})(\mu\text{-OAc})](ClO_4)\cdot H_2O\cdot(CH_3)_2CHOH$ (**2**) were determined by X-ray crystallography. The complex $[Cu_2(\mathbf{L3})(\mu\text{-OAc})]^{2+}$ [**3**; **L3** = *N*-(2-hydroxybenzyl)-*N*′,*N*′,*N*-tris(2-pyridylmethyl)-1,3-propanediamin-2-ol] was included in this study for comparison purposes only (Neves et al. *Inorg. Chim. Acta* **2005**, *358*, 1807−1822). Magnetic data show that the Cu^{II} centers in **1** and **2** are antiferromagnetically coupled and that the difference in the exchange coupling *J* found for these complexes ($J = -4.3$ cm^{-1} for **1** and $J = -40.0$ cm^{-1} for **2**) is a function of the Cu−O−Cu bridging angle. In addition, **1** and **2** were tested as catalysts in the oxidation of the model substrate 3,5-di-*tert*-butylcatechol and can be considered as functional models for catechol oxidase. Because these complexes possess labile sites in their structures and in solution they have a potential nucleophile constituted by a terminal Cu^{II}-bound hydroxo group, their activity toward hydrolysis of the model substrate 2,4-bis(dinitrophenyl)phosphate and DNA was also investigated. Double electrophilic activation of the phosphodiester by monodentate coordination to the Cu^{II} center that contains the phenol group with *tert*-butyl substituents and hydrogen bonding of the protonated phenol with the phosphate O atom are proposed to increase the hydrolase activity ($K_{ass.}$ and $k_{cat.}$) of **1** and **2** in comparison with that found for complex **3**. In fact, complexes **1** and **2** show both oxidoreductase and hydrolase/nuclease activities and can thus be regarded as man-made models for studying catalytic promiscuity.

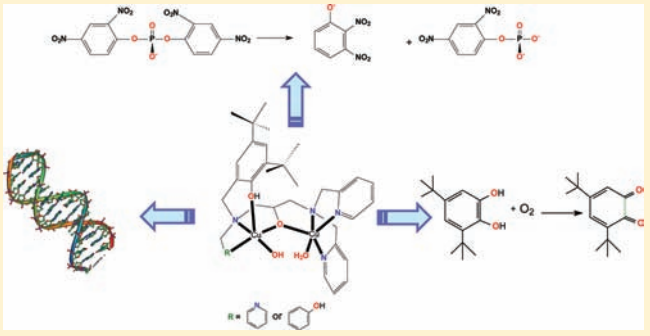

INTRODUCTION

Currently, much of the information regarding the role of metals in natural systems is gained through comparative studies on metalloenzymes and model metal complexes. For example, dinuclear hydrolytic and oxidative metalloenzymes, such as purple acid phosphatases (PAPs) and catechol oxidases (COs), respectively, have been used as appropriate starting points in the development of specific classes of synthetic metal complexes, known as synthetic hydrolases and/or chemical

Received: August 27, 2011
Published: January 19, 2012

nucleases, when mimicking PAPs,[1−13] catecholases,[1,14−31] and CO. Indeed, studies with model complexes have been described, aiming to mimic the structural and/or functional properties of these metalloenzymes, such as the intermetallic distance, asymmetry, and geometry around each metal center, with the presence of labile sites essential for binding of the substrate and/or available nucleophiles to initiate the catalytic process. In this way, through structural and spectroscopic analysis, as well as detailed reactivity studies on model compounds in solution, it is possible to propose the most probable mechanism involved in the catalytic process under investigation. In some cases, such information can be very helpful in clarifying the most probable mechanism associated with the native enzyme.[4,14,22]

In the active sites of numerous metalloenzymes, two adjacent metal centers act cooperatively in the transformation of substrate molecules. This is particularly true for biological oxidase or oxygenase activity involving molecular oxygen (O_2), in which the metal ions serve to activate the kinetically inert O_2 and the combined redox power of the two metal ions is used to mediate and to control the multielectron redox reactions. In view of the great importance of oxidation reactions in industrial and synthetic processes and of the ongoing search for new and efficient oxidation catalysts, it is of paramount interest to elucidate the basic functional principles that govern such bimetallic reactivity of natural enzymes.[32]

Dicopper sites play a pivotal role in biological oxygen chemistry and, consequently, understanding the structural and functional aspects of copper metalloenzymes is a subject of intensive research. A prominent member of these copper proteins is CO, which features a type 3 center with two proximate Cu atoms.

CO, also known as *o*-diphenol oxidase or polyphenol oxidase, catalyzes the two-electron-transfer reaction during the oxidation of a broad range of *o*-diphenols to the corresponding *o*-quinones by O_2. The resulting highly reactive quinones autopolymerize to form brown polyphenolic catechol melanins, a process thought to protect the damaged plant from pathogens or insects.[33−36] Although the high specificity of this reaction is of great importance for the determination of hormonal catecholamines (adrenaline, noradrenaline, and dopamine) in medical diagnoses, little is known about the mechanism of COs, beyond the availability of the three-dimensional structures of a CO from sweet potato (ibCO), which has been determined for the oxidized Cu^{II}−Cu^{II} state and the reduced Cu^{I}−Cu^{I} form.[33−36]

On the other hand, there is great interest in the development of new dinuclear model complexes that are able to mimic the catalytic properties of hydrolases/nucleases, a class of metalloenzymes that catalyze the hydrolysis of proteins, activated phosphodiesters, and DNA or RNA.[1−13] Although a great number of natural hydrolases are known, the search for small molecules able to cleave diester bonds in models and DNA molecules has been attracting special attention in attempts to identify the mechanism of the cleavage reactions, as well as their applicability as synthetic restriction enzymes, conformational probes, and catalysts.[37]

On the basis of the structural and physicochemical properties of natural enzymes, the principles postulated by Sargeson and co-workers[12] in the design of nucleophilic catalysts, and the concept of catalytic promiscuity for models recently described by Neves et al.,[15] we describe herein the syntheses, structure, physicochemical properties, and catecholase- and phosphatase-like activities of two dinuclear copper(II) model complexes. The unsymmetric dinucleating ligands (**L1** and **L2**) utilized in the syntheses of complexes **1** and **2** and the **L3** ligand are shown in Chart 1. The design of the ligands containing phenol groups with *tert*-butyl substituents was introduced based on the structure and properties of $[Cu_2(\mathbf{L3})(\mu\text{-OAc})]^{2+}$ (**3**),[6] in order to obtain dinuclear copper(II) complexes with distinct Lewis acidities and, consequently, distinct catecholase- and hydrolase-like activities. Interestingly, while complex **1** has been used as an efficient electrochemical sensor for the determination of hydroquinone in cosmetics,[38] complex **2** has been employed as a biomimetic sensor for catechin determination in green tea samples.[39]

Chart 1. Unsymmetric Dinucleating Ligands

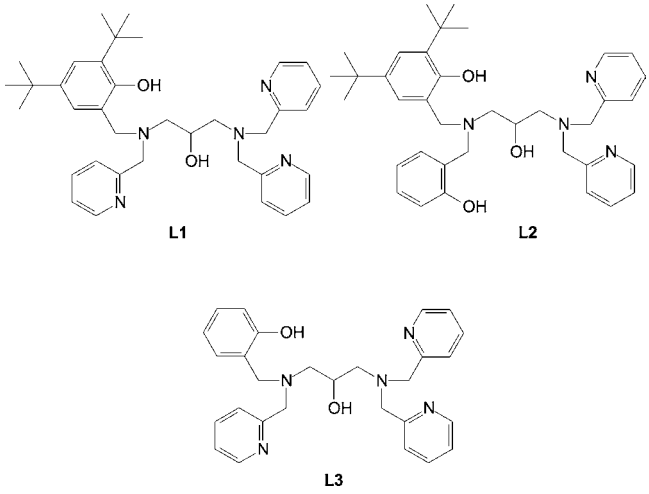

EXPERIMENTAL SECTION

The abbreviations used are as follows: **L1** = *N*′,*N*′,*N*-tris(2-pyridylmethyl)-*N*-(2-hydroxy-3,5-di-*tert*-butylbenzyl)-1,3-propanediamin-2-ol; **L2** = *N*′,*N*′-bis(2-pyridylmethyl)-*N*,*N*-(2-hydroxybenzyl)(2-hydroxy-3,5-di-*tert*-butylbenzyl)-1,3-propanediamin-2-ol; **L3** = *N*-(2-hydroxybenzyl)-*N*′,*N*′,*N*-tris(2-pyridylmethyl)-1,3-propanediamin-2-ol; **L4** = bis(2-hydroxybenzyl)-*N*-*N*′-bis(2-pyridylmethyl)-1,3-propanediamin-2-ol; 2,4-BDNPP = bis(2,4-dinitrophenyl)phosphate; 2,4-DNPP = 2,4-dinitrophenyl phosphate; 3,5-DTBC = 3,5 di-*tert*-butylcatechol.

Materials and Measurements. *N*′,*N*′,*N*-tris(2-pyridylmethyl)-1,3-propanediamin-2-ol,[6] *N*,*N*-bis(2-pyridylmethyl)-1,3-propanediamin-2-ol,[6] 2-(chloromethyl)-4,6-di-*tert*-butylphenol,[40] 2,4-BDNPP,[41] and 2,4-DNPP[42] were synthesized as previously described. Other reagents, materials, gases, and solvents of analytical or spectroscopic grade (in the kinetic studies and characterization of complexes) were purchased from commercial sources and used without further purification.

The plasmid pBSK II (2961 bp), used for DNA cleavage assays, was purchased from Stratagene, transformed into DH5a *Escherichia coli* competent cells, and amplified as previously described by Ausubel et al.[43] The plasmid DNA was extracted from *E. coli* and purified using Qiagen Plasmid Maxi Kit protocol.[44]

Physical Measurements. Elemental analyses were performed on a Carlo Erba E-1110 instrument. IR spectra were recorded on a Perkin-Elmer model FTIR-2000 spectrometer, using KBr pellets, in the range of 4500−450 cm^{-1}. Electronic absorption spectra in the 200−1200 nm range were recorded on a Perkin-Elmer Lambda 19 spectrophotometer. Electron paramagnetic resonance (EPR) spectroscopy analyses were performed in solid-state and frozen solutions at 77 K on a Bruker EMX spectrophotometer operating at a frequency of around 9.5 GHz (X-band), precisely determined, with a modulation frequency of 100 kHz, amplitude modulated from 2.024 G, and

dx.doi.org/10.1021/ic201876k | Inorg. Chem. 2012, 51, 1569−1589

microwave power of approximately 20 mW. ^{1}H NMR analysis was carried out using a Bruker 200 MHz spectrometer with $CDCl_3$ as the solvent, at room temperature. Chemical shifts were referenced to tetramethylsilane.

Electrochemical measurements were obtained using a Princeton Applied Research model 273 potentiostat/galvanostat. Square-wave voltammograms were obtained for the complexes in acetonitrile solutions containing 0.1 mol·L^{-1} tetrabutylammonium hexafluorophosphate as the supporting electrolyte under an argon atmosphere. The electrochemical cell employed was of a standard three-electrode configuration: platinum working electrode, platinum wire counter electrode, Ag/AgCl reference electrode. The Fc^+/Fc couple (E_0 = 400 mV vs NHE) was used as the internal standard.[45]

Electrospray ionization mass spectrometry (ESI-MS) of the complexes dissolved in an ultrapure acetonitrile/water (1:1, v/v) solution (500 μL) was analyzed using an amaZon X Ion Trap MS instrument (Bruker Daltonics) with an ion spray source using electrospray ionization in positive-ion mode. The ion source condition was an ion spray voltage of 4500 V. Nitrogen was used as the nebulizing gas (20 psi) and curtain gas (10 psi). The samples were directly infused into the mass spectrometer at a flow rate of 300 μL/h. The scan range was m/z 200−3000.

Magnetic Measurements and Theoretical Calculations of Magnetic Coupling. Magnetic susceptibility data were obtained in the temperature range of 2−300 K and in a magnetic field of 1000 Oe with a SQUID magnetometer on slightly pressed polycrystalline samples of complexes **1** and **2**. Diamagnetic corrections were applied in the usual manner with use of the tabulated Pascal's constants.[46]

The calculations described herein were performed at the density functional theory (DFT) level using Lee, Yang, and Parr's correlation functional B3LYP,[47] a hybrid functional including exact HF (Hartree−Fock) exchange in the ratio proposed by Becke.[48] All calculations employed the TZVPP basis set of Weigend and Ahlrichs for copper,[49] described as 17s11p6d1f, with the full contraction scheme to 842111/6311/411/1, and the Dunning's DZP basis set[50] for all other elements, which for carbon, oxygen, and nitrogen is described as 9s5p1d, with the full contraction scheme to 6111/41/1, and hydrogen is described as 4s1p contracted to 31/1.

Potentiometric Titration. Potentiometric studies were carried out with a Corning-350 research pH meter fitted with blue-glass and Ag/AgCl reference electrodes, calibrated to read −log [H$^+$] directly, designated as the pH, in ethanol/water (70:30, v/v). Potentiometric studies of complexes **1** and **2** were made in an ethanol/water mixture, instead of acetonitrile/water (as in the hydrolase experiments), because of the low solubility of the complexes in this media and need of higher concentrations for titration experiments.

Equilibrium measurements were performed in a thermostatted cell, purged with argon, containing 50.00 mL of the ethanol/water (70:30) solution and 0.02 mmol of the complex. The temperature was 25.00 ± 0.05 °C, and the experimental solutions were adjusted to 0.100 mol·L^{-1} of ionic strength by the addition of KCl. Computations of the triplicate results were carried out with the *BEST7*[51] program, and species diagrams were obtained with the *SPE*[51] and *SPEPLOT*[51] programs.

Reactivity. Catecholase- and hydrolase-like activities of complexes **1** and **2** were determined through oxidation of the model substrate 3,5-di-*tert*-butylcatechol (3,5-DTBC) and hydrolysis reaction of the model substrate 2,4-BDNPP,[41] respectively, under excess substrate conditions. The experiments were carried out, in triplicate, and monitored on a Varian Cary50 Bio spectrophotometer connected to a PC computer by following the increase in the 3,5-di-*tert*-butylquinone absorption band at 400 nm (ε = 1900 L·mol^{-1}·cm^{-1}) characteristic of oxidation reactions. For the hydrolase-like activity, the increase in the 2,4-dinitrophenolate characteristic absorption band at 400 nm (pH/ε L·mol^{-1}·cm^{-1} = (3.5/2125, 4.0/3408, 4.5/7182, 5.0/10 078, 5.5/11 405, 6.0/12 004;[52] 6.5−10.0/12 100)[53] was followed. Reactions were monitored to less than 5% conversion of the substrate, and the data were treated using the initial rate method, in the first 15 min of the reaction.

Initially, pH-dependent studies were carried out to determine the pH value at which catecholase- or phosphatase-like activities reached a maximum. The influence of the catecholase-like activity pH on the reaction rate for oxidation of 3,5-DTBC catalyzed by complexes **1** and **2** was determined over the pH range of 5.5−9.0 at 25 °C. To a quartz cell were added 100 μL of an aqueous solution ($[B]_{final}$ = 3.00 × 10^{-2} mol·L^{-1}) of buffer [MES (pH 5.5−6.5) and TRIS (pH 7.0−9.0)], 100 μL of a methanolic complex solution ($[C]_{final}$ = 2.40 × 10^{-5} mol·L^{-1}), and 3000 μL of air-saturated methanol. The reaction was initiated with the addition of 100 μL of a methanolic substrate solution ($[3,5\text{-DTBC}]_{final}$ = 5.00 × 10^{-3} mol·L^{-1}) and monitored for 15 min. The kinetic experiments under conditions of excess substrate were performed as follows: A total of 100 μL of aqueous buffer TRIS at pH 8.5 ($[B]_{final}$ = 3.00 × 10^{-2} mol·L^{-1}), 100 μL of a methanolic complex solution ($[C]_{final}$ = 2.40 × 10^{-5} mol·L^{-1}), and air-saturated methanol (from 2860 to 3076 μL, to complete 3300 μL) were added to a 1-cm-path-length cell at 25 °C. The reaction was initiated with the addition of known volumes (from 24 to 240 μL) of a 3,5-DTBC solution ($[3,5\text{-DTBC}]_{final}$ = 1.20 × 10^{-3}−12.00 × 10^{-3} mol·L^{-1}). To take into account the spontaneous oxidation of the substrate, correction was carried out using a reference cell under identical conditions but without the addition of the catalyst. The initial rate was obtained from the slope of the absorbance versus time plot over the first 15 min of the reaction. The Michaelis−Menten model was applied and the kinetic parameters were obtained from nonlinear square fits using the program *Origin 6.0*.

To detect the formation of hydrogen peroxide (or water) during the catalytic reaction, we employed a modified version of the iodometric method.[32] Reaction mixtures were prepared as in the kinetic experiments. After 1 h of reaction, an equal volume of water was added and the quinone formed was extracted three times with dichloromethane. The aqueous layer was acidified with H_2SO_4 (5.00 × 10^{-3} mol·L^{-1}) to pH 2 to stop further oxidation, and 1 mL of a 10% solution of KI and 3 drops of a 3% solution of ammonium molybdate were added. In the presence of hydrogen peroxide, the reaction $H_2O_2 + 2I^- + 2H^+ \rightarrow 2H_2O + I_2$ occurs and, with an excess of iodide ions, the triiodide ion is formed according to the reaction $I_2(aq) + I^- \rightarrow I_3^-$. The reaction rate is slow but increases with increasing concentrations of acid, and the addition of an ammonium molybdate solution renders the reaction almost instantaneous. The formation of I_3^- can be monitored spectrophotometrically because of the development of the characteristic band at 353 nm (ε = 26 000 L·mol^{-1}·cm^{-1}).[32]

Kinetic experiments for hydrolysis of 2,4-BDNPP were performed in aqueous/buffer media. Studies on the effects of the pH on the hydrolysis reaction were performed in the pH range of 3.50−10.00 at 50 °C. Reactions were performed using the following conditions: A total of 1500 μL of an aqueous solution ($[B]_{final}$ = 0.05 mol·L^{-1}) of buffer [MES (pH 3.50−6.50), HEPES (pH 7.00−8.50), and CHES (pH 9.00−10.00)] (I = 0.05 mol·L^{-1} $LiClO_4$), 200 μL of an acetonitrile complex solution ($[C]_{final}$ = 4.00 × 10^{-5} mol·L^{-1}), and 1000 μL of acetonitrile were added to a 1-cm-path-length cell. The reaction was initiated with the addition of 300 μL of an acetonitrile substrate solution ($[2,4\text{-BDNPP}]_{final}$ = 5.00 × 10^{-3} mol·L^{-1}) and monitored for 15 min.

Under conditions of excess substrate, 200 μL of an acetonitrile solution of the complex ($[C]_{final}$ = 4.00 × 10^{-5} mol·L^{-1}) was added to 1500 μL of an aqueous buffer solution [HEPES (pH 8.00)] ($[B]_{final}$ = 5.00 × 10^{-2} mol·L^{-1}) and acetonitrile (from 480 to 1520 μL, to complete 3300 μL). The reaction was initiated with the addition of known volumes (80−1120 μL) of a 2,4-BDNPP solution ($[2,4\text{-BDNPP}]_{final}$ = 5.00 × 10^{-4}−7.00 × 10^{-3} mol·L^{-1}). Corrections for the spontaneous hydrolysis of 2,4-BDNPP were accomplished by a direct difference using a reference cell under identical experimental conditions, without adding the catalyst.

In order to establish the number of molecules of substrate that are hydrolyzed per molecule of complex, the reaction was monitored at 445 nm (ε = 3600 L·mol^{-1}·cm^{-1}), under a 50-fold substrate excess ($[2,4\text{-BDNPP}]_{final}$ = 2.00 × 10^{-3} mol·L^{-1}), relative to the complex ($[C]_{final}$ = 4.00 × 10^{-5} mol·L^{-1}), at pH 8.00 and 50 °C. The stoichiometric reactions ($[C]_{final}$ = 4.00 × 10^{-5} mol·L^{-1} and

dx.doi.org/10.1021/ic201876k | *Inorg. Chem.* 2012, 51, 1569−1589

$[2,4\text{-BDNPP}]_{final} = 4.00 \times 10^{-5}$ mol·L^{-1}) were also monitored (400 nm) to investigate the possible hydrolysis of the monoester 2,4-DNPP, one of the products from the hydrolysis reaction of the diester 2,4-BDNPP, at pH 8.00 and 50 °C.

DNA Cleavage Activity. The ability of **1**and **2** to cleave DNA was examined by following the conversion of supercoiled plasmid DNA (FI) to the open-circular DNA (FII) and/or linear DNA (FIII) forms using agarose gel electrophoresis to separate the cleavage products. In general, 330 ng of pBSK II (25 μmol·L^{-1} in pb) in PIPES (pH 6.0 and 7.0), HEPES (pH 8.0), or CHES (pH 9.0) buffer was treated with different concentrations of **1**and **2** in CH_3CN (25% in reaction volume) for 6 h at 37 °C. Thereafter, each reaction was quenched by adding 5 μL of a loading buffer solution (0.01% bromophenol blue, 50% glycerol, and 250 mM EDTA, pH 8.0) and the sample subjected to electrophoresis on a 0.8% agarose gel containing 0.3 μg·mL^{-1} of ethidium bromide in a 0.5TBE buffer (44.5 mmol·L^{-1} TRIS, 44.5 mmol·L^{-1} boric acid, and 1 mmol·L^{-1} EDTA) at 90 V for about 1.5 h. The resulting gels were visualized and digitalized with a Gel Logic 200 gel documentation system (Carestream Health, USA). The proportion of DNA in each band was quantified using KODAK Molecular Imaging Software 5.0 (Carestream Health, USA). The proportion of supercoiled DNA was corrected by a factor of 1.47 because the ability of ethidium bromide to intercalate into this topoisomeric form is decreased relative to the circular and linear forms.[54]

To elucidate the mechanism involved in the DNA cleavage performed by **1** and **2**, different cleavage inhibitors were added to the DNA prior to the complex. The reactive oxygen species (ROS) scavengers dimethyl sulfoxide (DMSO; 10%), KI (500 μmol·L^{-1}), superoxide dismutase (SOD; 20 units), and NaN_3 (500 μmol·L^{-1}) were used in order to identify the presence of ROS during the DNA scission event. In addition, assays in the presence of a copper(I) stabilizer, bathocuproine (500 μmol·L^{-1}), the minor groove binder distamycin (50 μmol·L^{-1}), and the major groove binder methyl green (50 μmol·L^{-1}) were also performed. The plasmid DNA was pretreated with distamycin and methyl green for 30 min and treated with the complex as described above. Furthermore, the influence of the ionic strength on DNA cleavage was evaluated using several concentrations (0−200 mmol·L^{-1}) of sodium chloride (NaCl).

The rates of DNA cleavage (k_{obs}) by **1** and **2** were determined by treating the plasmid DNA at different complex concentrations (0−200 μmol·L^{-1} to **1** and 0−25 μmol·L^{-1} to **2**) for different intervals of time (0−6 h). The k_{obs} values were calculated for each complex concentration, assuming pseudo-first-order kinetics, and then analyzed following the pseudo-Michaelis−Menten formalism.[55] The reaction conditions were the same as those described above.

Syntheses of the Ligands and Complexes 1 and 2. Detailed experimental procedures for the preparation of the ligands **L1** and **L2** and their dinuclear perchlorate complexes **1** and **2**, respectively, have been reported elsewhere.[38,39]

Caution! *Perchlorate salts of metal complexes are potentially explosive and therefore should be prepared in small quantities.*

Single-Crystal X-ray Structure Determinations. Blue crystals for complexes **1** and **2** were selected, and crystallographic analyses were carried out with an Enraf-Nonius CAD4 diffractometer with graphite-monochromated Mo Kα radiation (λ = 0.710 69 Å), at room temperature. Cell parameters were determined from 25 carefully centered reflections. Intensities were collected using the $\omega-2\theta$ scan technique. All data were corrected for Lorentz and polarization effects. A semiempirical absorption correction based on the azimuthal scans of seven appropriate reflections was also applied to the collected intensities. The structures were solved by direct methods and refined by full-matrix least-squares methods using the *SIR97*[56] and *SHELXL97*[57] programs, respectively. H atoms attached to C atoms were placed at their idealized positions, with C−H distances and U_{eq} values taken from the default settings of the refinement program. The figures for the molecular structures were produced with the *PLATON*[58] program. Further crystallographic information for these complexes are described below and summarized in Table 1.

Complex **1**. A prismatic blue crystal was selected for X-ray analysis. The crystals of complex **1** showed very poor scattering power. From 17 443 collected intensities, 16 884 are unique and just 7240 are observed. Even so, the structure was solved, and two conformational isomers of **1**, four perchlorate counterions, and two isopropyl alcohol solvate molecules were found in the asymmetric unit. All perchlorate ions are disordered, in which O atoms occupy two alternative positions. Two *tert*-butyl groups are also disordered, with two partial occupancies for each terminal C atom. All non-H atoms were refined with anisotropic displacement parameters, except for disordered *tert*-butyl groups and perchlorate counterions, which were refined isotropically. H atoms of the isopropyl alcohol solvate were found from Fourier difference map and treated with riding model.

Complex **2**. The crystallographic data were acquired from a selected prismatic blue crystal token from the crystalline sample. Non-H atoms were refined with anisotropic displacement parameters. H atoms of the phenol group and water molecules were found from a Fourier map treated with a riding model. H atoms of the isopropyl alcohol solvate could not be located from a difference Fourier map maybe because its O atom was found to be disordered.

Table 1. Crystallographic Data for Complexes 1 and 2

	1	2
empirical formula	$C_{41}H_{57}Cl_2Cu_2N_5O_{13}$	$C_{42}H_{59}ClCu_2N_4O_{11}$
fw (g·mol^{-1})	1025.90	958.46
temperature (K)	293(2)	293(2)
wavelength (Å)	0.710 69	0.710 69
cryst syst	triclinic	triclinic
space group	$P\bar{1}$	$P\bar{1}$
unit cell dimens	a = 15.041(1) Å	a = 11.287(1) Å
	b = 18.556(1) Å	b = 12.001(1) Å
	c = 20.663(1) Å	c = 18.518(5) Å
	α = 66.485(6)°	α = 95.935(5)°
	β = 68.511(6)°	β = 99.886(5)°
	γ = 72.333(7)°	γ = 110.484(7)°
volume (Å^3)	4836.2(5)	2278.3(7)
Z, calcd density (g·cm^{-3})	4/1.409	2/1.397
cryst size (mm^3)	0.50 × 0.26 × 0.16	0.60 × 0.26 × 0.20
abs coeff (mm^{-1})	1.054	1.053
F(000)	2136	1004
θ range for data collection (deg)	2.17−25.10	2.14−25.07
index ranges	$-17 \le h \le 16$, $-22 \le k \le 0$, $-24 \le l \le 22$	$-12 \le h \le 13$, $-14 \le k \le 0$, $-21 \le l \le 22$
reflns collected/ unique	17 443/16 884 [R(int) = 0.0418]	8509/8089 [R(int) = 0.0178]
abs corrn	ψ scan	ψ scan
max and min transmn	0.9523 and 0.8214	0.9712 and 0.8774
refinement method	full-matrix least squares on F^2	full-matrix least squares on F^2
data/restraints/ param	16 884/289/1119	8089/108/579
GOF on F^2	1.022	1.050
final R indices [$I > 2\sigma(I)$]	R1 = 0.0733, wR2 = 0.1912	R = 0.0404, R_w = 0.0999
R indices (all data)	R1 = 0.2336, wR2 = 0.2450	R = 0.0854, R_w = 0.1134
largest diff peak and hole (e·Å^{-3})	0.942 and −0.676	0.443 and −0.340

RESULTS AND DISCUSSION

Syntheses. The ligands **L1** and **L2** (Chart 1) were obtained with sufficient purity and yields for use without further purification in the synthesis of the dinuclear copper(II) complexes **1** and **2**.[38,39] The unsymmetrical dinucleating ligands presenting two potentially different tridentate pendant arms allowed one to obtain the dinuclear

dx.doi.org/10.1021/ic201876k | Inorg. Chem. 2012, 51, 1569−1589

$[Cu_2(\mathbf{L1})(\mu\text{-OAc})](ClO_4)_2\cdot(CH_3)_2CHOH$ (**1**) and $[Cu_2(\mathbf{L2})(\mu\text{-OAc})](ClO_4)\cdot H_2O\cdot(CH_3)_2CHOH$ (**2**) complexes in which the metal centers reside in distinct coordination environments and geometries (vide infra). The perchlorate salts of **1** and **2** were obtained in good yields by reacting respectively the ligands **L1** and **L2** with $Cu(OAc)_2\cdot H_2O$ (1:2) in methanol in the presence of a stoichiometric amount of $NaClO_4\cdot 3H_2O$. Recrystallization from a CH_2Cl_2/isopropyl alcohol (1:1) solution of **1** and a isopropyl alcohol solution of **2** afforded crystals of both complexes suitable for X-ray crystallographic analysis.

X-ray Structural Characterization. Complex **1** crystallizes as single blue crystals belonging to the triclinic crystal system and space group $P\bar{1}$. The asymmetric unit of this complex consists of two molecules of **1**. Because the bond lengths and angles and the geometry around the Cu^{II} centers are identical in the two molecules (**1** and **2**), only the parameters of molecule **1** will be discussed here. An ORTEP view of the cation complex is presented in Figure 1. The crystallographic data and the main bond distances/angles are given in Tables 1 and 2, respectively.

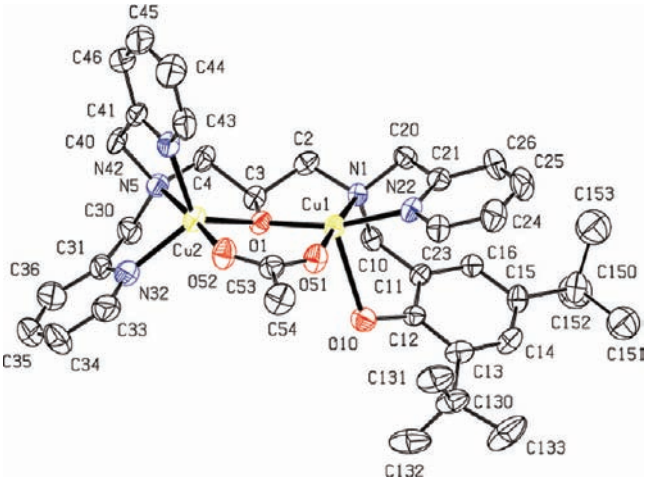

Figure 1. ORTEP[58] view of the cation complex $[Cu_2(\mathbf{L1})(\mu\text{-OAc})]^{2+}$–**1**.

Table 2. Main Bond Distances (Å) and Angles (deg) for Complex 1

Cu1–O1	1.892(5)	Cu2–O52	1.922(7)
Cu1–N22	1.948(7)	Cu2–O1	1.943 (5)
Cu1–O51	1.957(6)	Cu2–N42	2.070(7)
Cu1–N1	2.025(6)	Cu2–N32	2.078(9)
Cu1–O10	2.470(6)	Cu2–N5	2.033(7)
Cu1–Cu2	3.3975(15)		
O1–Cu1–N22	164.5(3)	O52–Cu2–N5	176.0(3)
O1–Cu1–O51	96.0(3)	O1–Cu2–N5	84.4(3)
N22–Cu1–O51	94.1(3)	O52–Cu2–N42	98.0(3)
O1–Cu1–N1	86.4(2)	O1–Cu2–N42	121.3(3)
N22–Cu1–N1	83.7(3)	N5–Cu2–N42	82.1(3)
O51–Cu1–N1	177.5(3)	O52–Cu2–N32	95.5(3)
O1–Cu1–O10	101.4(2)	O1–Cu2–N32	123.7(3)
N22–Cu1–O10	90.2(2)	N5–Cu2–N32	80.8(3)
O51–Cu1–O10	90.2(2)	N42–Cu2–N32	110.0(3)
N1–Cu1–O10	88.6(2)	Cu1–O1–Cu2	124.7(3)
O52–Cu2–O1	98.9(3)	C12–O10–Cu1	110.5(5)

Figure 1 shows the structure of the cation complex **1**, which is composed of one unsymmetric **L1** ligand coordinated to both Cu^{II} centers (Cu1 and Cu2). Each Cu^{II} center is five-coordinated and is bridged by the alkoxo donor O atom of the ligand and by an exogenous acetate ion.

The Cu1 center is five-coordinated, having a square-pyramidal geometry as determined by the τ value (0.22).[59] The basal plane is composed of the amine N1 atom, the pyridinic N22 atom, and the alkoxo O1 and acetate O51 bridging atoms. The protonated phenol O10 atom is in the apical position of the square pyramid with $Cu-OH_{phenol}$ = 2.470(6) Å and completes the N_2O_3 coordination sphere of Cu1.

The geometry around the Cu2 center (N_3O_2-donor set) is best described as distorted trigonal-bypiramidal with τ = 0.87.[59] In the trigonal plane, the Cu2 atom is coordinated by the pyridinic N32 and N42 atoms and the alkoxo bridging O1 atom. The amine N5 atom and the acetate bridging O52 atom are in the pseudoaxial positions, completing the five-coordination sphere of Cu2 with an O52–Cu2–N5 bond angle of 176.0(3)°.

The bond distances and angles observed in **1** and **2** are in agreement with those found in copper(II) complexes with a μ-alkoxo bridge and nonequivalent geometries around the metallic centers, coordinated by similar N,O-donor groups.[8,60] The main difference between complexes **1** and **3**[8] is the presence of *tert*-butyl groups in **1**, localized in the positions ortho and para to the phenolic O atom, which should cause an increase in the electron density over the Cu1 center.[8] In fact, the $Cu1-O_{phenol}$ distance in **1** is only slightly shorter [2.470(6) Å] than the corresponding distance observed in **3** [2.504(10) Å].[8]

Complex **2** crystallizes as prismatic blue crystals that belong to the triclinic crystal system and space group $P\bar{1}$. An ORTEP view of the cation complex $[Cu_2(\mathbf{L2})(\mu\text{-OAc})]^+$ is presented in Figure 2. The crystallographic data and the main bond distances and angles are given in Tables 1 and 3, respectively.

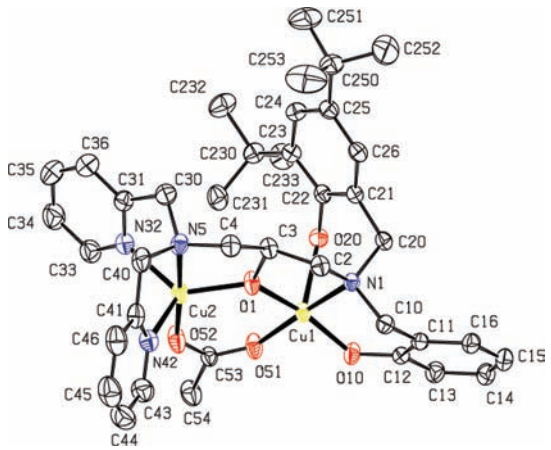

Figure 2. ORTEP[58] view of the cation complex $[Cu_2(\mathbf{L2})(\mu\text{-OAc})]^+$–**2**.

In complex **2**, the Cu1 center is five-coordinated, showing a square-pyramidal geometry as determined by the τ value (0.11).[59] The phenolic O20 atom containing the *tert*-butyl groups is protonated and is coordinated in the apical position of the pyramid with $Cu-OH_{phenol}$ = 2.455(2) Å in agreement with a Jahn–Teller distortion observed in copper complexes.

dx.doi.org/10.1021/ic201876k | Inorg. Chem. 2012, 51, 1569–1589

Table 3. Main Bond Distances (Å) and Angles (deg) for Complex 2

Cu1−O1	1.897(2)	Cu2−O52	1.916(2)
Cu1−O10	1.902(2)	Cu2−O1	1.937(2)
Cu1−O51	1.977(2)	Cu2−N5	2.017(3)
Cu1−N1	2.042(2)	Cu2−N32	2.092(3)
Cu1−O20	2.455(2)	Cu2−N42	2.118(3)
Cu1−Cu2	3.4837(6)		
O1−Cu1−O10	167.93(11)	O52−Cu2−N5	177.14(10)
O1−Cu1−O51	92.77(9)	O1−Cu2−N5	84.82(10)
O10−Cu1−O51	85.66(10)	O52−Cu2−N32	96.63(12)
O1−Cu1−N1	85.54(9)	O1−Cu2−N32	127.79(11)
O10−Cu1−N1	94.90(10)	N5−Cu2−N32	81.53(11)
O51−Cu1−N1	174.50(11)	O52−Cu2−N42	97.26(12)
O1−Cu1−O20	96.26(9)	O1−Cu2−N42	117.52(11)
O10−Cu1−O20	95.80(9)	N5−Cu2−N42	81.37(12)
O51−Cu1−O20	98.00(9)	N42−Cu2−N32	109.80(11)
N1−Cu1−O20	87.39(9)	Cu1−O1−Cu2	130.67(11)
O52−Cu2−O1	98.04(9)	C12−O10−Cu1	126.5(2)

This coordination mode is comparable to those observed in **1** and in complexes **3** and $[Cu_2(\mathbf{L4})(\mu\text{-OAc})(H_2O)_2]^{2+}$ in which the $Cu-OH_{phenol}$ distances are respectively 2.470(6), 2.504(10),[8] and 2.433(10) Å.[60]

The tertiary amine N1 atom, the phenolate O10 atom, and the O51 and O1 atoms from the acetate and alkoxo bridges, respectively, compose the basal plane of the square pyramid. The $Cu-O_{phenolate}$ [Cu1−O10 = 1.902(2) Å] bond distance is similar to those observed for other phenolate complexes containing Cu^{II},[61−64] and the other phenolic O20 atom completes the five-coordinated environment around the Cu1 center.

The coordination environment around the Cu2 center is similar to that observed in **1** with a tendency toward a distorted trigonal-bipyramidal geometry, as reflected by the structural index parameter τ of 0.83. The Cu atom is coordinated to three N and two O atoms: the pyridine N atoms (N32 and N42), the tertiary amine N atom (N5), and the acetate and μ-alkoxo O atoms (O52 and O1), respectively. Finally, with an increase in the Cu···Cu distance in **2** [3.4837(6) Å] compared to **1** [3.3975(15) Å], there is a concomitant opening of the Cu−O(alkoxo)−Cu angle from 124.7(3)° in **1** to 130.67(11)° in **2**.

Magnetic Properties. The variable-temperature magnetic data for complexes **1** and **2** in the solid state, collected in the temperature range of 2−300 K and in a magnetic field of 1000 Oe, are shown in Figure 3 and indicate a distinct degree of coupling between the Cu^{II} centers in these complexes. For complex **1**, the effective magnetic moment ($\mu_{eff} = 2.828[\chi_{mol}T]^{1/2}$) per 2Cu is approximately constant (~2.70 μ_B) in the temperature range of 300−16 K and then decreases more rapidly to 1.62 μ_B at 2 K. On the other hand, for complex **2**, μ_{eff} per 2Cu decreases gradually from 2.60 μ_B at 300 K to 2.3 μ_B at 60 K and then decreases more rapidly to 1.63 μ_B at 2 K. The data were fitted by the exact diagonalization of the spin Hamiltonian

$$\mathcal{H} = -J\cdot S_1\cdot S_2 + \mu_B[(g_1\cdot S_1 + g_2\cdot S_2) + 2\rho S]\mathbf{H} - zJ'\langle S_z\rangle(S_{1z} + S_{2z}) \quad (1)$$

where S_1 and S_2 are spin operators of the copper dimer, S is a copper monomer impurity spin, ρ is an impurity fraction, **H** is the magnetic field, and the last term in the Hamiltonian presents intermolecular interaction in the molecular-field approximation. The values calculated for susceptibility were powder-averaged. Fits obtained are shown in Figure 3. There was essentially no improvement in the fit when the anisotropy of the exchange and intermolecular interactions was taken into account. In particular, it was not possible to obtain a good fit for complex **1** with $J > 0$ by $zJ' < 0$. The results obtained from the fits are consistent with those obtained by applying the formula of Bleaney and Bowers, modified with respect to the presence of impurities.[65] The parameters obtained are listed in Table 4, together with the data of other dinuclear $[Cu^{II}(\mu\text{-alkoxo})(\mu\text{-OAc})Cu^{II}]$ complexes described in the literature.[16,60,66]

The X-ray structures of complexes **1** and **2** reveal that the Cu1 centers have square-pyramidal geometry in which the unpaired electron is in the $d_{x^2-y^2}$ magnetic orbital, while both Cu2 centers have trigonal-bipyramidal geometry, with the unpaired electron localized in the d_{z^2} magnetic orbital (Figures 1 and 2, respectively). Indeed, a great number of dinuclear copper(II) complexes containing the structural $[Cu^{II}(\mu\text{-alkoxo})(\mu\text{-carboxylato})Cu^{II}]$ unit have been structurally and magnetically characterized.[16,23,26,67−69] However, with a few exceptions,[8,28,70,71] most of these complexes have been obtained with symmetrical dinucleating alkoxo and phenoxo

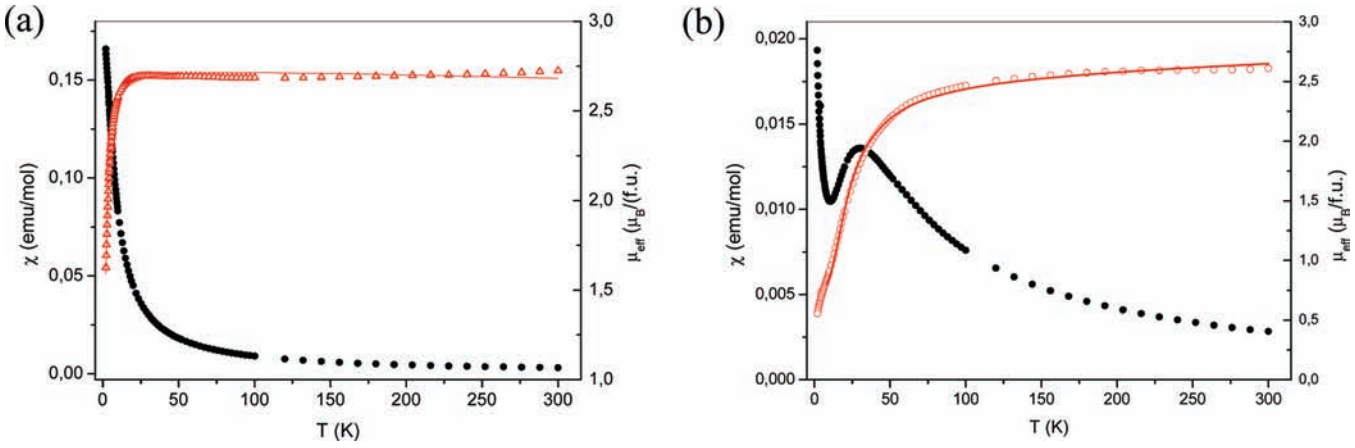

Figure 3. Temperature dependence of χ_M (◆) and μ_{eff} (○) for complexes **1** (a) and **2** (b).

dx.doi.org/10.1021/ic201876k | Inorg. Chem. 2012, 51, 1569−1589

Table 4. Magnetic and Structural Data for Complexes 1 and 2 and Other Complexes Described in the Literature

complex	g	TIP ($cm^3 \cdot mol^{-1}$)	J (cm^{-1})	% impurity	Cu···Cu (Å)	Cu−O−Cu (deg)
1	2.01	$\sim 210 \times 10^{-6}$	−4.3	6.9	3.397	124.7
2	2.11	$\sim 350 \times 10^{-6}$	−40	7.5	3.483	130.66
4[16]	2.075		−78	3.0	3.511	132.85
5[16]	2.0		−76	1.5	3.517	131.7
6[16]	2.062		43		3.159	108.08
7[16]	2.01		77.6		3.081	104.76
8[66]	2.04	40.0×10^{-6}	26		3.239	114.4
9[66]	2.007	60.0×10^{-6}	16.7		3.286	114.3
10[60]	2.1	60.0×10^{-6}	−25	5.7	3.400	127.9

ligands, but even so, they revealed a significant range of interesting structural and magnetic properties. For instance, it has been assumed that in the [Cu^{II}(μ-alkoxo)(μ-carboxylato)Cu^{II}] unit μ-acetate cannot promote coupling between the Cu^{II} ions[72] and that differences in the magnetic behavior of these systems can be rationalized using the "ligand orbital complementary" concept.[66,73,74] In addition, it has been concluded that dinuclear copper(II) complexes containing both $d_{x^2-y^2}$ and d_{z^2} magnetic ground states show ferromagnetic coupling because of the orthogonality of the magnetic orbitals.[75]

For the complexes described herein, the weak antiferromagnetic coupling between the Cu^{II} centers in **1** ($J = -4.3$ cm^{-1}) is in agreement with the fact that the μ-alkoxo group can interact with the unpaired electron in the $d_{x^2-y^2}$ orbital around Cu1, but it does not overlap with the orbital having the unpaired electron in the d_{z^2} orbital (Cu2), which is oriented toward the acetate bridging group, as shown in Figure 4. On the other hand,

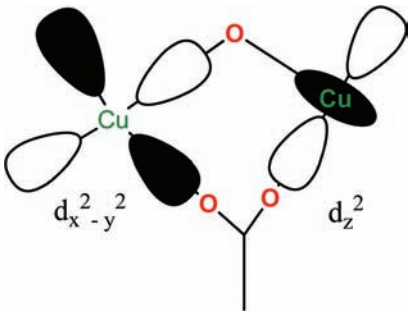

Figure 4. Schematic representation of the orientation of orbitals in complexes **1** and **2**.

complex **2** shows a significantly higher antiferromagnetic interaction ($J = -40$ cm^{-1}) between the Cu^{II} centers compared to complex **1**, and such a phenomenon has not been observed previously for [Cu^{II}(μ-alkoxo)(μ-carboxylato)Cu^{II}] complexes in which the magnetic ground states of the Cu1 and Cu2 centers are respectively $d_{x^2-y^2}$ and d_{z^2}. In fact, magnetic interactions between the metal centers in dinuclear copper(II) complexes are strongly structure-dependent, and in the present study, precise structural and magnetic data for complexes **1** and **2** are available. On the basis of the structure of **2**, it can be concluded that the geometry around Cu1 is only slightly distorted ($\tau = 0.11$) from a square-pyramidal structure. Thus, the dominant magnetic orbital of Cu1 appears to be the $d_{x^2-y^2}$ orbital. On the other hand, it is anticipated that distortion in the coordination geometry around the Cu2 center ($\tau = 0.83$) and the greater bridging Cu−O−Cu angle (θ) of 130.66° in **2** compared to 124.7° in complex **1** could lead to some mixing of the d_{z^2} orbital associated with the trigonal-bipyramidal geometry with the $d_{x^2-y^2}$ ground state of the square pyramid, thus giving rise to stronger antiferromagnetism ($J = -40$ cm^{-1}) in **2**. Alternatively, it could be speculated that the acetate bridging group is able to interact with the unpaired electron on each Cu^{II} ion by direct overlap. However, the weak antiferromagnetic coupling observed for **1** indicates that the contribution of the carboxylate group to the exchange mechanism should be minor compared with that of the μ-alkoxo ligand.[75]

Wei and co-workers[16] have established that the magnitude of the exchange integral in dinuclear copper(II) complexes containing the [Cu^{II}(μ-alkoxo)(μ-carboxylato)Cu^{II}] structural unit is a linear function of the Cu−O−Cu bridging angle; the exchange is ferromagnetic below 116.5° and antiferromagnetic above this value. Interestingly, according to the modified plot presented by Wei et al. given in Figure 5 (θ vs J instead of θ vs $2J$)

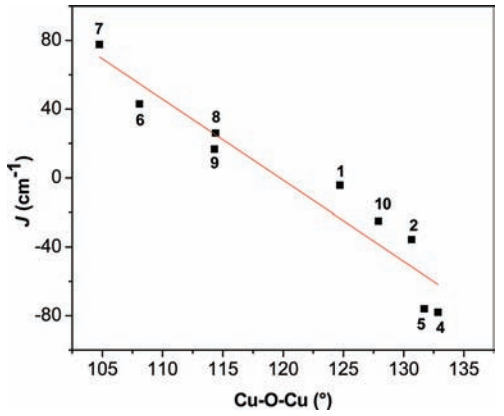

Figure 5. Exchange integral (J) versus Cu−O−Cu (θ) bridge angle for [Cu^{II}(μ-alkoxo)(μ-OAc)Cu^{II}] complexes. The numbers next to the points represent the compounds. See references for complexes **4**−**10** in Table 4.

and including **1** and **2**, it becomes apparent that the difference in the exchange coupling J found for these complexes is also a function of the Cu−O−Cu bridging angle, as was already established for other [Cu^{II}(μ-alkoxo)(μ-carboxylato)Cu^{II}] complexes.[16] Moreover, this conclusion is also supported by theoretical calculations for complex **2**, which show that the computed J value obtained from the fully optimized structure is in excellent agreement with the experimental antiferromagnetic coupling constant.

Study of the Magnetic Coupling Constants *J* for 1 and 2 Obtained by Theoretical Calculations. The interaction between two paramagnetic metallic centers can be quantified by the sign and magnitude of the isotropic magnetic exchange

dx.doi.org/10.1021/ic201876k | Inorg. Chem. 2012, 51, 1569−1589

coupling constant, J, based on the most commonly used spin Hamiltonian, the so-called HDVV (Heisenberg–Dirac–van Vleck) spin Hamiltonian (eq 1a).[76]

$$H_{HDVV} = -JS_1S_2 \quad (1a)$$

where S_1 and S_2 denote the individual spin operators of the two metallic centers. DFT, combined with the broken-symmetry (BS) approach, was adopted in our calculations of the magnetic interaction between the Cu^{II} centers in complexes **1** and **2**. In fact, the BS formalism has been proven to be an efficient and practical alternative to elucidate the magnetic exchange couplings of dinuclear transition-metal systems.[77−80]

The magnetic exchange coupling constant J was evaluated using three different equations:

$$J^{(1)} = -\frac{E_{HS} - E_{BS}}{(S_1 + S_2)^2} \quad (2)$$

$$J^{(2)} = -\frac{E_{HS} - E_{BS}}{(S_1 + S_2)(S_1 + S_2 + 1)} \quad (3)$$

$$J^{(3)} = -\frac{E_{HS} - E_{BS}}{\langle S^2\rangle_{HS} - \langle S^2\rangle_{BS}} \quad (4)$$

where E_{HS} and E_{BS} are the energies of the high-spin (HS) and BS configurations, respectively.

All calculations reported here were performed using the *ORCA Quantum Chemical Program*.[81] To understand the structural effects on the computed coupling constant, we performed three different types of calculations. First, we simply used the crystallographic structures of complexes **1** and **2** and added H atoms to complete the valences of the atoms. Second, we optimized only the positions of the H atoms and allowed the remainder of the molecular skeleton to be fixed. Third, we considered the full system and optimized the structure with no geometry or symmetry constraints. In the latter case, the geometry was optimized considering only the low-spin (LS) state because a previous study[80] showed that a better agreement between the magnetic susceptibility measurements and the computed magnetic coupling constant is obtained when the LS geometry is used. Neese and co-workers[79] also noted that the use of the LS geometry to compute J seems to be more appropriate because the electron density of the LS state corresponds to the electron density of the real antiferromagnetic state. The magnetic coupling constants computed are given in Table 5.

Table 5. Magnetic Exchange Coupling Constants, J, in cm^{-1}, Calculated for Complexes 1 and 2 Using the B3LYP Functional[a]

	1			2		
	A1	A2	A3	A1	A2	A3
$J^{(1)}$	6.96	0.47	−19.51	−19.41	−30.66	−39.08
$J^{(2)}$	3.48	0.23	−9.76	−9.70	−15.33	−19.54
$J^{(3)}$	6.94	0.47	−19.39	−19.28	−30.44	−38.55
$J^{exp.}$	−4.3	−40				

[a]A1: using the X-ray structures of **1** and **2**. A2: using the X-ray structures of **1** and **2** and optimizing only the positions of the H atoms. A3: using the fully optimized geometry.

As can be seen, the exchange coupling constants calculated using the different approaches shown in eqs 2−4 show similar trends. For example, the values for the magnetic exchange interaction between the two Cu^{II} ions calculated using the X-ray structure of complex **2** are −19.41, −9.70, and −19.28 cm^{-1} for $J^{(1)}$, $J^{(2)}$, and $J^{(3)}$, respectively. When the positions of the H atoms are optimized, these values change to −30.66, −15.33, and −30.44 cm^{-1}. An excellent agreement between the computed $J = -38.55$ cm^{-1} and the experimental $J = -40$ cm^{-1} is obtained when the structure is fully optimized, which shows the dependence of the coupling constant on the structural parameters.

The computed coupling constant of complex **1** calculated using the X-ray structure showed that the two Cu^{II} ions are ferromagnetically coupled. This is in contrast with the experimental findings, which suggest that the Cu^{II} centers are antiferromagnetically coupled ($J = -4.3$ cm^{-1}). Nevertheless, when the J constant is determined using the fully optimized structure, the coupling behavior is correctly described; however, the results are not quantitatively correct. This disagreement between calculated and experimental data of the magnetic coupling constant of **1** can be explained by the fact that the optimized structure does not faithfully represent the experimental structure. Some optimized geometrical parameters for compounds **1** and **2** are shown in Table 6.

Table 6. Selected Geometrical Parameters for Complexes 1 and 2 Calculated Using the B3LYP Functional[a]

structural parameter	1	2
Cu1−Cu2	3.530(3.397)	3.560(3.484)
Cu1−O1	1.909(1.892)	1.901(1.897)
Cu2−O1	1.971(1.943)	2.018(1.937)
∠Cu1−O1−Cu2	130.9(124.7)	130.5(130.7)

[a]Experimental X-ray values are given in parentheses. Distances are given in angstroms and angles in degrees.

As can be seen in Table 6, there is a good agreement between the calculated and experimental parameters for complex **2**. In general, the difference between the calculated and experimental distances is less than 0.08 Å, while the difference in the Cu−O−Cu angle is only 0.2°. However, for complex **1**, the difference between the calculated and experimental Cu−O−Cu angles is 6°, thus distorting the structure and making the calculated angle identical in both structures. This finding suggests that the deviation of this angle is most probably responsible for the disagreement between the computed and experimentally observed coupling constants and indicates that the μ-alkoxo bridge is directly involved in the coupling process. Again, as discussed in the interpretation of the experimental J values for complexes **1** and **2** (vide supra), it can be concluded that the Cu−O−Cu angle probably plays the most important role in determining the degree and sign of the magnetic coupling in these $[Cu^{II}(\mu\text{-alkoxo})(\mu\text{-carboxylato})Cu^{II})]$ complexes.

Table 7 shows the spin density (ρ) values for both complexes in their HS and BS states. Only the spin densities at the metallic atoms, the O atom of the μ-alkoxo bridge, and the μ-caboxylate atoms are quoted. The positive and negative signs indicate α and β spin densities, respectively. As can be seen, the spin density at the Cu1 center remains constant at around 0.6 for both complexes, in their HS and BS spin states, compared to the formal electron counting value of 1.0. In the BS state, the spin density at the Cu2 center, as expected, is inverted, and the magnitude of the β spin density is almost equivalent to those of

dx.doi.org/10.1021/ic201876k | *Inorg. Chem.* 2012, 51, 1569−1589

Table 7. Mulliken Spin Densities for Complexes 1 and 2

atom	1	2
	HS State	
Cu1	0.596	0.578
Cu2	0.618	0.621
O1	0.131	0.130
C53	−0.006	−0.007
O51	0.055	0.081
O52	0.115	0.093
	BS State	
Cu1	0.588	0.580
Cu2	−0.610	−0.615
O1	−0.007	0.037
C53	0.004	−0.001
O51	0.054	0.078
O52	−0.113	−0.092

the α spin densities computed in the HS state. The bridging O atom also has a small α spin density in the HS state, which is reduced in the BS state, indicating that the bridge is involved in the magnetic coupling mechanism. It is noteworthy that the O atom of the μ-caboxylate ligand has a small α spin density in the HS state, which is inverted at O52 in the BS state, suggesting that the carboxylate group may be involved in the coupling mechanism. However, the spin density at the C atom of the carboxylate group is negligible, which, in turn, avoids overlap with the p orbitals of the O atoms.

Figure 6 shows plots of the corresponding orbitals[82,83] of the magnetic electrons, involved in the exchange coupling mechanism, for compounds **1** and **2**. For both complexes, only one exchange pathway, with reasonable overlap, is found. From inspection of the figure, we can see that the exchange pathway can be described as a σ/π pathway involving the in-plane alkoxo p orbitals and the metal d orbitals. As can be seen, the p orbitals of the O atoms of the carboxylate group overlap with the d orbitals of the metal sites. However, there is no participation of the p orbitals of the C atoms of the carboxylate group, which makes this group an inefficient mediator of the superexechange interactions and, thus, the contribution of the carboxylate group to the exchange mechanism is minor compared with the μ-alkoxo ligand. These results indicate that the exchange interaction in the coumpounds studied is mediated preferentially by the superexchange mechanism via the O atoms of the μ-alkoxo bridge.

Electronic Spectroscopy, EPR, and Electrochemical Properties. The electronic spectrum of **1** in an acetonitrile solution (Figure 7, solid line) shows a band centered at 698 nm (ε = 169 L·mol^{-1}·cm^{-1}) and one at 890 nm (ε = 194 L·mol^{-1}·cm^{-1}), which are typical of Cu^{II} d−d transitions. A further band at 482 nm (ε = 225 L·mol^{-1}·cm^{-1}) can be attributed to a ligand-to-metal charge transfer (LMCT) between the phenolate and the Cu^{II} ions. This suggests that in solution an equilibrium between the protonated and deprotonated coordinated phenols is most probably taking place. It is important to mention here that the reflectance spectrum of **1** in the solid state does not show this band.

On the other hand, complex **2**, in an acetonitrile solution (Figure 7, dotted line), shows only one wide band centered at 700 nm (ε = 370 L·mol^{-1}·cm^{-1}), typical of Cu^{II} d−d transitions,

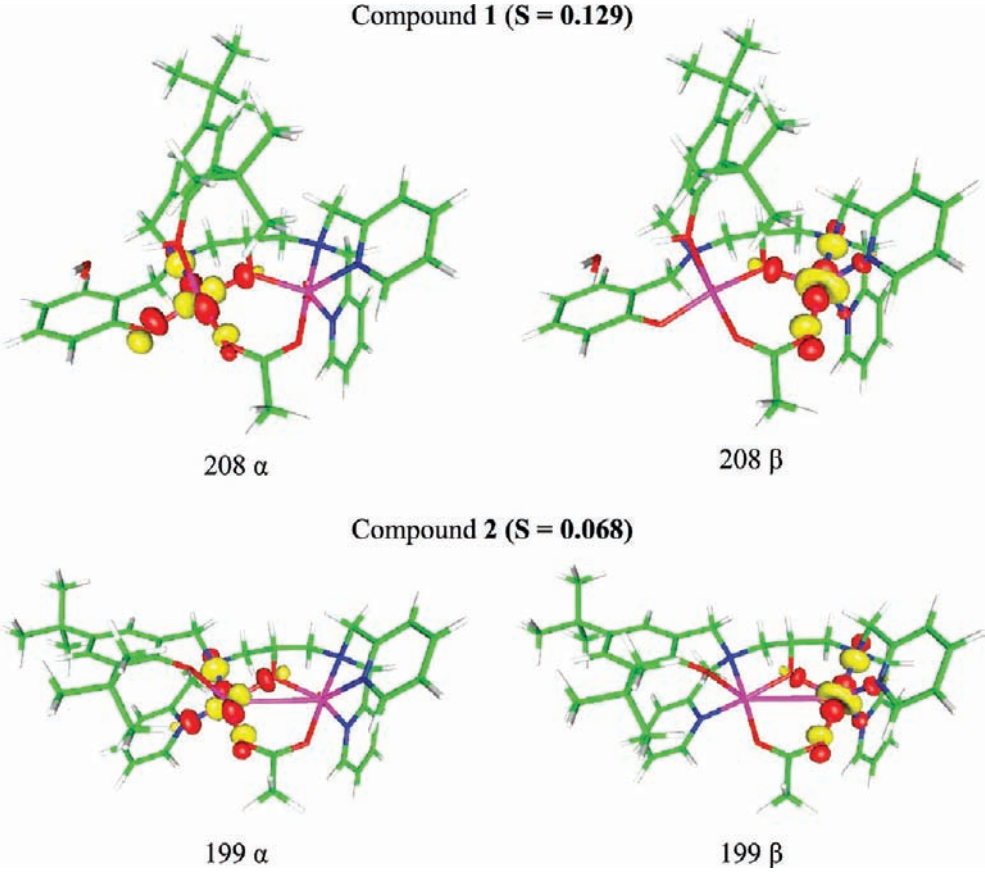

Figure 6. Magnetic orbitals of compounds **1** and **2** (the orbital number is quoted).

dx.doi.org/10.1021/ic201876k | Inorg. Chem. 2012, 51, 1569−1589

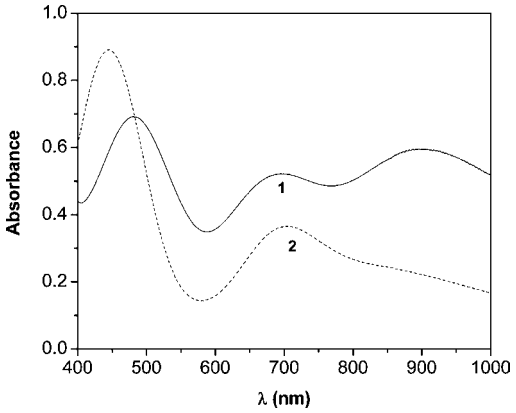

Figure 7. Electronic spectra of **1** (solid line) and **2** (dotted line). Concentrations: **1** (1.0×10^{-3} mol·L^{-1}) and **2** (3.0×10^{-3} mol·L^{-1}) in acetonitrile.

and another one at 446 nm (ε = 900 L·mol^{-1}·cm^{-1}) attributed to a LMCT of the type between equatorial phenolate to Cu^{II} ions, which is in full agreement with X-ray structure characterization. In fact, the spectrum of **2** is very similar to that obtained for **1**, but with the band observed in the 850–950 nm range being less defined for **2**. The reflectance spectrum of **2** in the solid state is very similar to that observed in acetonitrile, indicating that the coordination environment around the Cu^{II} centers is maintained when complex **2** is dissolved in solution.

The X-band EPR spectra of solid samples of **1** and **2** at 77 K are shown in Figure 8. Complex **1** shows a typical axial spectrum with four well-defined lines ($g_{\|} > g_{\perp} > 2.0$), and the following parameters were obtained from the simulated spectrum: $g_{\|}$ = 2.265, $g_{\perp}$ = 2.056, $A_{\|} = 175 \times 10^{-4}$ cm^{-1}, and $A_{\perp} = 22 \times 10^{-4}$ cm^{-1}.

The spectrum also shows an additional signal, although not well-defined, at the half-field transition (1500 G), which can be assigned to the forbidden transition $\Delta M_s = \pm 2$. These data suggest that the two Cu^{II} ions are antiferromagnetically coupled, as demonstrated through magnetic measurements.

Similarly, under identical conditions, the spectrum of complex **2** shows a less defined fine structure for $\Delta M_s = \pm 1$, and the following parameters were obtained from the simulated spectrum: $g_{\|}$ = 2.245, $g_{\perp}$ = 2.07, $A_{\|} = 191 \times 10^{-4}$ cm^{-1}, and $A_{\perp} = 15 \times 10^{-4}$ cm^{-1}. However, in complex **2**, there is a stronger Cu–Cu interaction, evidenced by a well-defined and intense signal at the half-field transition $g \cong 4.3$. Such behavior is consistent with a singlet–triplet splitting (interaction between metallic centers) with weak antiferromagnetic coupling, and thus the spectra of both complexes, including the difference in intensity, are in full agreement with the magnetic coupling constants J obtained by magnetic measurements (vide supra). In addition, the microcrystalline EPR spectra of **1** and **2** are similar to those observed for other dinuclear $Cu^{II}Cu^{II}$ complexes in which the Cu^{II} centers are weakly antiferromagnetically or ferromagnetically coupled.[8,28,84] Nevertheless, it is important to mention here that, for the few described examples of dinuclear Cu^{II} systems containing the unpaired electron in both $d_{x^2-y^2}$ and d_{z^2} magnetic orbitals, EPR spectra do not show the proposed d_{z^2} ground state for copper.[75]

The electrochemical behavior of the compounds was studied using square-wave voltammetry. The square-wave voltammograms for **1** and **2** are shown in Figure S1 in the Supporting Information. A solution of **1** in acetonitrile displays a *quasi*-reversible process at E_{pc1} = −388 mV vs NHE, corresponding to the $Cu^{II}Cu^{II}/Cu^{II}Cu^{I}$ redox couple, and another irreversible process at E_{pc2} = −788 mV vs NHE, originating from the $Cu^{II}Cu^{I}/Cu^{I}Cu^{I}$ process. The square-wave voltammogram of **2** shows a similar behavior, with cathodic processes at E_{pc1} = −560 mV and E_{pc2} = −1083 mV vs NHE, corresponding to the same reduction processes. The reduction potentials observed for complexes **1** and **2** are in full agreement with those reported in the literature for complex **3**[22] but with E_{pc} values being anodically shifted (Table 8). Complex **3** is structurally similar to complex **1**, without *tert*-butyl groups localized in the positions ortho and para to the phenolic donor O atom.

Table 8. Electrochemical Data for Complexes 1–3

complex	E_{pc1} mV vs NHE	E_{pc2} mV vs NHE	$\Delta E_{(1,2)}$ mV vs NHE
1	−388	−788	400
2	−560	−1083	523
3[22]	−890	−1110	220

In fact, negative reduction potential is a tendency observed for dinuclear copper(II) complexes with μ-alkoxo bridge and phenolate ligands because of the electron density at the metal centers originating from the donor O atoms.[17,22]

Solution Studies: Potentiometric Titration, ESI-MS, and EPR. In order to establish the catalytically relevant species for catecholase-like activity and the hydrolysis of diester bonds, potentiometric titration, EPR, and ESI-MS studies were carried

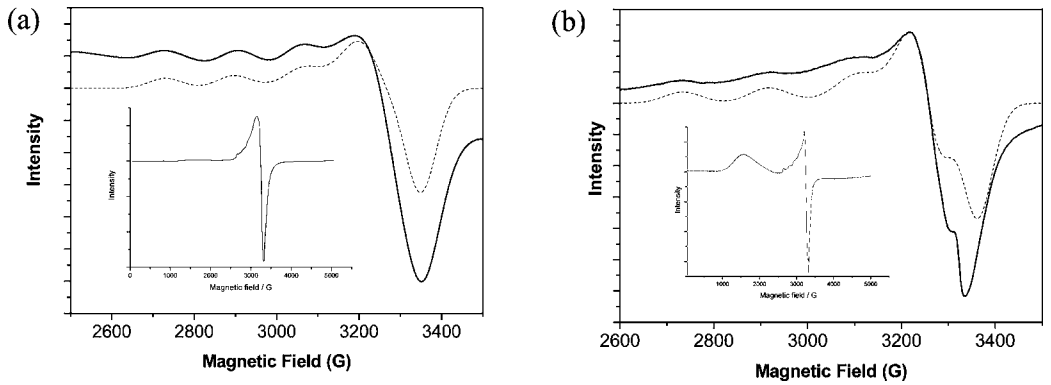

Figure 8. X-band EPR spectra for complexes **1** (a) and **2** (b) in the solid state at 77 K: —, experimental points; ---, simulated curve. Inset: EPR spectrum showing the $\Delta M_s = \pm 2$ transition.

dx.doi.org/10.1021/ic201876k | Inorg. Chem. 2012, 51, 1569–1589

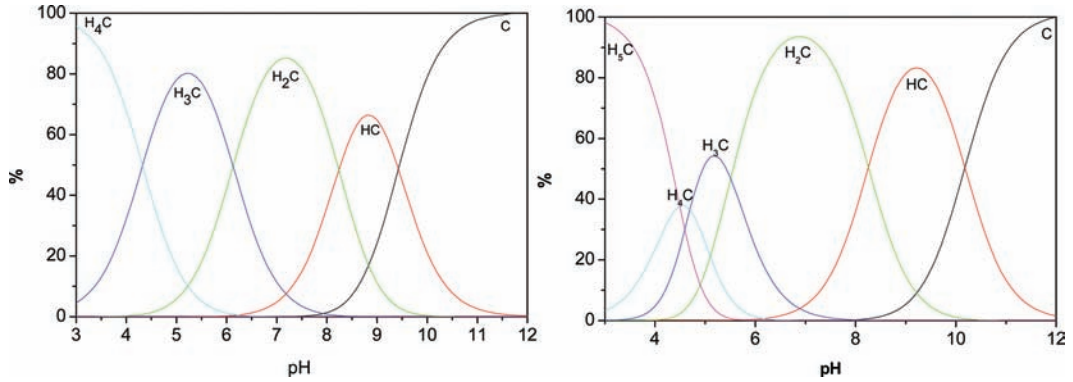

Figure 9. Species distribution curves of complexes **1** (left) and **2** (right) as a function of the pH, at 25 °C and I = 0.05 mol·L^{-1} (KCl).

Scheme 1. Deprotonation/Protonation Equilibrium Steps for Complex 1

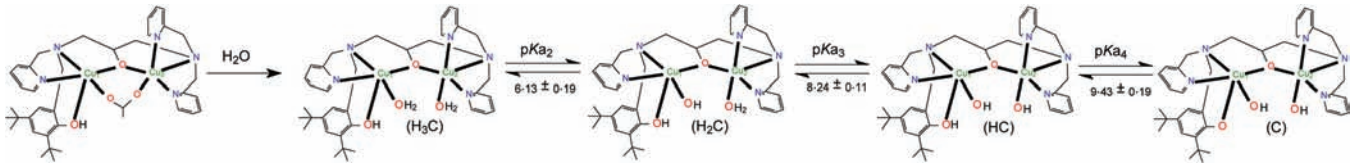

Scheme 2. Deprotonation/Protonation Equilibrium Steps for Complex 2

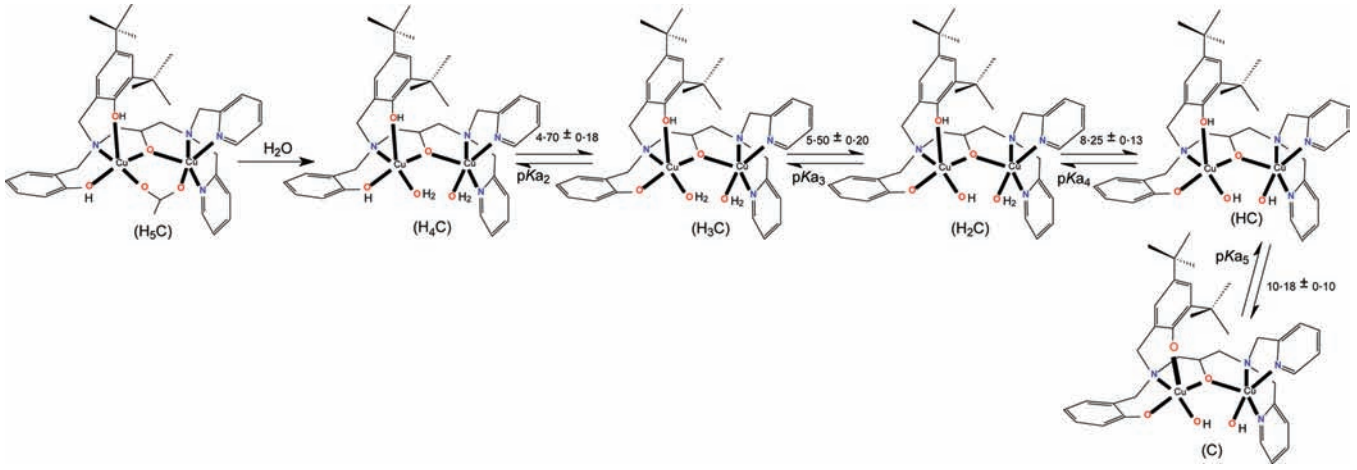

out in ethanol/water or CH_3CN/water solution. It is important to mention here that, although no potentiometric titration in a CH_3CN/water solution could be carried out for **1** and **2** (precipitation of the complexes), pK_a values obtained for other dinuclear complexes, in water/ethanol (30:70), are only ∼0.15 pH units lower than those in water/CH_3CN (50:50).[52]

Potentiometric titration of complexes **1** and **2** (Figures 9 and S2 in the Supporting Information) was carried out in ethanol/water (70:30), in order to compare the pK_a values obtained by potentiometric titration with those obtained from the kinetic experiments (hydrolase- and catecholase-like activities of **1** and **2**).

In ethanol/water (70:30), neutralization of 4 mol of KOH per 1 mol of complex **1** and 5 mol of KOH per 1 mol of complex **2**, in the pH range of 3.00−12.00, was obtained, and the deprotonation/protonation equilibrium steps and corresponding pK_a values are proposed in Schemes 1 and 2, respectively.

The pK_a values found for complex **1** are 4.32 ± 0.14, 6.13 ± 0.19, 8.24 ± 0.11, and 9.43 ± 0.19, and those for complex **2** are 4.49 ± 0.16, 4.70 ± 0.18, 5.50 ± 0.20, 8.25 ± 0.13, and 10.18 ± 0.10. When **1** and **2** are dissolved in aqueous solution (pH 3.0), for both complexes, dissociation of the acetate bridge with replacement by two water molecules to generate species H_3C and H_4C for **1** and **2**, respectively, is expected and strongly supported by the ESI-MS data (vide infra). Thus, pK_{a1} is attributed to the protonation/deprotonation equilibrium of the released acetate/acetic acid group for complexes **1** and **2**.

For complex **1**, H_2C has a water molecule coordinated to one Cu^{II} ion and a hydroxide ion coordinated to the other Cu^{II} ion; HC represents the complex with two hydroxide ions coordinated to the dinuclear centers, and C can be attributed to deprotonation of the terminal phenol group that is bound to the Cu1 center, as observed in the X-ray structure of **1**. In addition, the assignment of this species is in full agreement with that determined through spectrophotometric titration of **1** under identical experimental conditions (Figure S3 in the Supporting Information).

The pK_a values for complex **2** (4.49, 5.50, and 8.25) are attributed, respectively, to dissociation of the acetate bridge, a water molecule coordinated to one Cu^{II} ion, and a water molecule coordinated to the other Cu^{II} ion. These values are in

dx.doi.org/10.1021/ic201876k | Inorg. Chem. 2012, 51, 1569−1589

agreement with the protonation/deprotonation equilibrium described by Neves et al.[22] for dinuclear copper(II) complexes containing μ-alkoxo and terminal phenol/phenolate ligands. Assignment of the pK_a values 6.13 and 5.50, respectively, for **1** and **2**, to deprotonation of the water molecule bound to the Cu^{II} center containing the protonated phenol ligands is in agreement with the higher Lewis acidity of this center compared to the other Cu^{II} ions in the dinuclear complexes. In fact, this hypothesis is supported by the averaged Cu1−N,O/Cu2−N,O bond distances around the Cu^{II} ions, which are respectively 2.058/2.009 and 2.054/2.016 Å for **1** and **2**. On the other hand, it seems that the same argument is not apparent for the difference of ∼0.6 pH units observed between the corresponding dissociation constants in **1** and **2** because the averaged Cu1−N,O bond distances are similar in the two complexes. However, the electrochemical data (Table 9) are in full agreement with these results and reveal that the reduction potentials for **2** are anodically shifted by 172 and 295 mV compared to those for **1**, thus confirming the higher Lewis acidity of both Cu^{II} centers in complex **2**. Finally, H_3C and C represent the species resulting from deprotonation of the equatorial and axial phenol groups, respectively. These species were confirmed through spectrophotometric titration of **2** under experimental conditions identical with those employed in the potentiometric tritration experiments (Figure S3 in the Supporting Information).

Table 9. Kinetic Parameters for the Oxidation Reaction of 3,5-DTBC Catalyzed by Complexes 1−3 at pH 8.50 and 25 °C

complex	V_{max} ($mol \cdot L^{-1} \cdot s^{-1}$)	K_M ($mol \cdot L^{-1}$)	$k_{cat.}$ (s^{-1})	$K_{ass.}$ ($L \cdot mol^{-1}$)	$k_{cat.}/K_M$ ($M^{-1} \cdot s^{-1}$)
1	6.17×10^{-7}	3.47×10^{-3}	0.025	288.18	7.41
2	1.24×10^{-6}	9.44×10^{-3}	0.051	105.93	5.47
3[a]	1.90×10^{-7}	9.50×10^{-4}	0.0078	1000.0	8.10

[a] **3** represents the complex $[Cu_2(\mathbf{L3})(\mu\text{−OAc})]^{2+}$.[22]

ESI-MS measurements for **1** and **2** were recorded in CH_3CN/water (50:50), the same solvent conditions as those employed for kinetic assays. For complex **1**, three main group of peaks are observed at mass-to-charge (m/z) ratios of 864.19, 764.25, and 382.12 (Figure S4 in the Supporting Information). The peak at m/z 764.25 can be attributed to $[Cu^{II}Cu^{I}(\mathbf{L1})(CH_3CN)(OH_2)]^+$, indicating reduction of the Cu^{II} center coordinated by the soft side of the ligand ion under the conditions of the ESI-MS, while the peak at m/z 382.12 corresponds to the dication $[Cu^{II}Cu^{II}(\mathbf{L1})(CH_3CN)(OH_2)]^{2+}$. The peak at m/z 864.19 is assigned to the $[Cu^{II}Cu^{II}(\mathbf{L1})(CH_3CN)(OH_2)(ClO_4)]^+$ species. On the other hand, when complex **2** is submitted to ESI-MS, a prominent peak at m/z 779.25 can be observed (Figure S5 in the Supporting Information). This peak is assigned to the $[Cu^{II}Cu^{I}(\mathbf{L2})(CH_3CN)(OH_2]^+$ species (reduction of one Cu^{II} center) in which CH_3CN and H_2O molecules are probably added to the Cu^{II} centers during the ionization process as with complex **1**. It is important to emphasize that, for both complexes, there is no observation of acetato-bridged species under these conditions, in full agreement with the proposed protonation/deprotonation equilibrium from potentiometric titration (vide supra).

EPR spectra for complexes **1** and **2** were obtained in frozen CH_3CN/water (50:50) solutions, pH 7.0 at 77 K. The spectrum of **1** (Figure S6, top, in the Supporting Information) reveals that when the complex is dissolved in a CH_3CN/water (1:1) buffer solution at pH 7.0, the $g_{\|}/A_{\|}$ = 118 ratio is significantly decreased compared to that of the solid-state spectrum ($g_{\|}/A_{\|}$ = 129), a strong indication that the ligand field around the Cu^{II} centers is increased when OH^- groups are coordinated. Indeed, these results are in full agreement with the potentiometric data, which suggests that, under these experimental conditions, $[(OH)Cu^{II}Cu^{II}(OH_2)]$ (H_2C in Scheme 1) should be the main species present in solution. In addition, the spectrum of **1** shows a signal at the half-field transition ($g \cong 4.3$), characteristic of dinuclear $Cu^{II}Cu^{II}$ species with a weak antiferromagnetic coupling. Thus, it is reasonable to conclude that in solution the dinuclear $[(OH)Cu^{II}(\mu\text{-alkoxo})Cu^{II}(OH_2)]$ structural unit is present as the catalytic species (vide infra). The EPR results for complex **2** (Figure S6, bottom, in the Supporting Information) are similar to those presented for **1** and will not be discussed further in the manuscript.

Finally, for both complexes, the formation of a $Cu^{II}(\mu\text{-OH})Cu^{II}$ is disfavored most probably because of the rigid five-membered rings formed by coordination of the Cu^{II} ions to the 1,3-diaminopropan-2-ol moiety.[6] Detailed studies would require EPR measurements at other frequencies, which is outside the scope of the present work.

Reactivity. *Kinetic Studies for the Catecholase-Like Activity.* The catecholase-like activity of the dinuclear copper(II) complexes was determined by the catalytic oxidation of 3,5-DTBC. This substrate is most widely used because of its low redox potential, which facilitates oxidation to quinone, and its bulky substituents, which make further oxidation reactions, such as ring opening, slower.[85]

The kinetic studies of the oxidation of 3,5-DTBC by complexes **1** and **2** were carried out by the method of initial rates by monitoring the increase in the characteristic quinone (3,5-DTBQ) absorption band, which is sufficiently stable and displays a strong absorption band at 400 nm (ε = 1900 $L \cdot mol^{-1} \cdot cm^{-1}$), whose appearance was monitored by UV/vis spectroscopy over time. It was found that under anaerobic conditions only 1 equiv of 3,5-DTBQ is formed, and when oxygen is bubbled into the solution, the catalytic activity is regenerated, indicating that the catalyst is still active and that oxygen must participate directly in the catalytic cycle of the oxidation reaction, acting as a thermodynamic driving force by reoxidizing any copper(I) species and regenerating them to the active copper(II) species. Therefore, in all cases, the solvent was saturated with O_2 before the kinetic experiments. To correct for the effect of the spontaneous reaction, the same solution was used without adding the catalyst as an internal reference.

The dependence of the oxidation reaction catalyzed by complexes **1** and **2** on the pH was investigated within the range of 5.5−9.0 to determine the pH value at which the catecholase-like activity is at a maximum. For both complexes, a sigmoidal-shaped profile was obtained, as seen in Figure S7 in the Supporting Information. The data were fitted using a Boltzman model, and a sigmoidal fit of the curves revealed kinetic pK_a values of 8.0 ± 0.1 for complex **1** and 7.7 ± 0.1 for complex **2**, which are in relative good agreement with the pK_a values obtained from the potentiometric titrations; pK_a = 8.24 for **1** and pK_a = 8.25 for **2**. Indeed, these results suggest that deprotonation of a second water molecule coordinated to a Cu^{II} center in complexes **1** and **2** occurs to generate the active dihydroxo species (HC in Schemes 1 and 2) for the oxidation reaction of 3,5-DTBC. As was previously postulated for other

dx.doi.org/10.1021/ic201876k | Inorg. Chem. 2012, 51, 1569−1589

dinuclear copper(II) complexes described in the literature,[22] the pH dependence of the catalytic activity is most probably due to the fact that the Cu^{II}-coordinated hydroxo groups are able to interact with catechol, promoting deprotonation of the substrate and its bridging coordination to the metal centers. The activity of the enzyme is observed in the pH range of 5−8 (optimum at pH 7.8), with the loss of activity below pH 4.0 and above pH 9.0.[35]

Saturation kinetics were obtained at pH 8.5. The graph of the initial reaction rates (V_0) versus 3,5-DTBC concentrations shows a saturation profile (Figure 10). This dependence of the

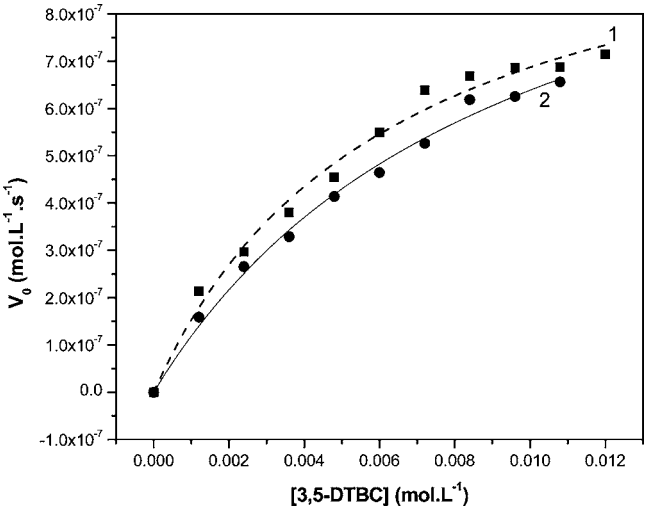

Figure 10. Dependence of the reaction rates on the 3,5-DTBC concentration for the oxidation reaction catalyzed by complexes **1** (■) and **2** (●), in a methanol/water (32:1 v/v) solution. Conditions: [complex] = 2.40×10^{-5} mol·L^{-1}; [3,5-DTBC] = $(1.20-12.00) \times 10^{-3}$ mol·L^{-1}; [buffer] = 3.30×10^{-2} mol·L^{-1} (TRIS, pH 8.50) at 25 °C.

rate on the substrate concentration suggests that the oxidation reaction occurs with the formation of an intermediate substrate/complex. The Michaelis−Menten model was applied, and the kinetic parameters were obtained from nonlinear square fits using the program *Origin 6.0*. The parameters V_{max}, K_M, and $k_{cat.}$ are shown in Table 9.

As can be observed in Table 9, complex **1** is more effective in the conversion of the substrate 3,5-DTBC to the corresponding *o*-quinone, with a catalytic efficiency of 7.41 L·mol^{-1}·s^{-1} compared to 5.47 L·mol^{-1}·s^{-1} found for complex **2**. This is a reflection of its association constant ($K_{ass.}$ = 288.2 L·mol^{-1}), which is around 3 times higher in comparison to that observed for complex **2**. Interestingly, the value of $K_{ass.} = 10^3$ L·mol^{-1} previously reported for **3** is around 4 and 10 times higher than those observed for **1** and **2**, respectively. It is important to emphasize that complex **3** corresponds to complex **1** without substituents at the phenolic donor atoms and complexes **1** and **2** have respectively 2+ and 1+ formal charges. Indeed, several factors must be considered in assessing the difference in the oxidation activities of complexes **1**−**3**, such as the association affinity, mode of interaction of substrate, electrochemical properties, exogenous donors, and steric match.[22] Thus, the difference in the association constants for complexes **1** and **2** can be attributed to the different formal charges in these catalysts, with $K_{ass.}$ being around 3 times higher for **1**, under identical experimental conditions (pH 8.5). On the other hand, it seems that the presence of bulky *tert*-butyl groups localized in the positions ortho and para to the phenolic donor O atom in **1** and **2** is responsible for the significant decrease in $K_{ass.}$ compared to **3**, and thus the formation of the intermediate substrate/complex would be inhibited by steric constraints caused by the ligand under kinetic conditions.

With respect to the catalytic turnover number ($k_{cat.}$), we found that the reactivity in the oxidation of 3,5-DTBC increases in the order **3** < **1** < **2**. From the electrochemical data given in Table 8, one can observe that there is a correlation between $k_{cat.}$ and the reduction potential values of complexes **1**−**3**. The more anodically shifted the individual E_{pc} values, the higher the catalytic turnover of the complex. Thus, as expected, complex **2**, which is the strongest oxidant within the series of catalysts, shows the highest $k_{cat.}$, while complex **3** has the lowest activity. In addition, we also found a good correlation between the electrochemical parameter $[(\Delta E)_{1,2} = E_{pc1} - E_{pc2}]$ and the catalytic efficiency ($k_{cat.}/K_M$) of complexes **1**−**3**, with complex **3** being the most efficient and complex **2**, which has the highest $k_{cat.}$, being the least efficient in the conversion of 3,5-DTBC to the corresponding *o*-quinone. In fact, as was previously emphasized by these authors,[22] $(\Delta E)_{1,2}$ is an important parameter because it represents how readily the metal centers accept the electron pair from the substrate in the oxidation reaction, while the correlation between $k_{cat.}/K_M$ and $(\Delta E)_{1,2}$ supports the mechanistic idea that a one-electron intermediate is disfavored in this two-electron reaction. Thus, one can conclude that despite the higher catalytic turnover of complex **2** it represents the less efficient catalyst in the oxidation of 3,5-DTBC, which can be attributed to its higher $(\Delta E)_{1,2}$ within the series of complexes **1**−**3**.

The accumulation of H_2O_2 during turnover was confirmed by means of the molybdate-accelerated I_3^- assay (75% of the expected amount was detected), which indicates that reoxidation of the copper(I) species back to the active copper(II) species occurs with a 1:1 O_2/3,5-DTBC stoichiometry and concomitant formation of hydrogen peroxide. The release of H_2O_2 is mechanistically distinct from the native COs.[86]

Finally, the catecholase-like activity was also studied in the absence of oxygen. The reaction was carried out under identical kinetic conditions, observed over 60 h at 25 °C, and only 1 equiv of quinone was found, which demonstrated that oxygen must participate in the catalytic cycle of the oxidation reaction by reoxidizing any Cu^I back to the active Cu^{II} species.

In summary, the combined experimental data support a mechanistic model for the oxidation reaction of 3,5-DTBC catalyzed by **1** and **2**, as given in Figure 11. At pH 8.5, in the first step of the reaction, we propose that the dihydroxo $[(OH)Cu^{II}Cu^{II}(OH)]$ complex is able to interact with catechol, promoting deprotonation of the substrate and coordination to the Cu^{II} centers and forming the adduct complex/substrate. Next, an intramolecular electron-transfer reaction, as the rate-determining step, results in oxidation of the catechol substrate to the corresponding *o*-quinone and reduction of the Cu^{II} centers to Cu^I. The Cu^ICu^I complex in the presence of O_2 is immediately oxidized back to the original form, hydrogen peroxide is formed, and the catalytic cycle is completed.

It is important to note that the release of H_2O_2 observed in the oxidation of 3,5-DTBC by **1** and **2** is mechanistically distinct from the type III dinuclear enzyme COs.[86] On the other hand, the proposed mechanism (Figure 11) resembles that of the copper-loaded form of S100B in which the catalytic

dx.doi.org/10.1021/ic201876k | *Inorg. Chem.* 2012, 51, 1569−1589

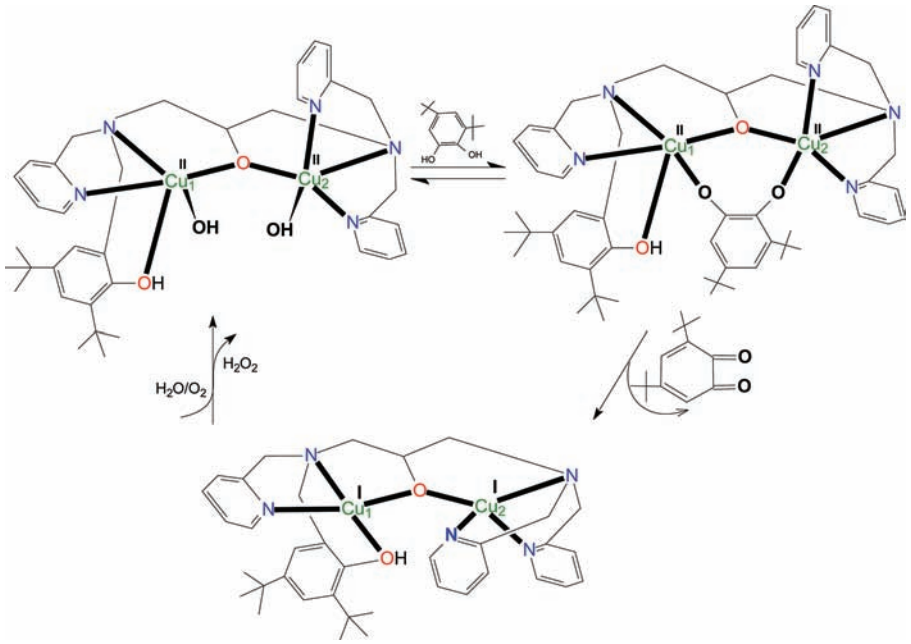

Figure 11. Proposed mechanism for the oxidation of 3,5-DTBC catalyzed by complex **1**. The mechanism proposed for **2** is similar.

two-electron oxidation of catechols is initiated by two strongly coupled Cu^{II} centers and the release of H_2O_2.

Kinetic Studies for the Hydrolase-Like Activity. Kinetic experiments were carried out to assess the ability of complexes **1** and **2** to catalyze hydrolysis of the substrate 2,4-BDNPP. Under excess substrate conditions, the experiments were performed in triplicate and spectrophotometrically monitored at 400 nm (pH/ε $L{\cdot}mol^{-1}{\cdot}cm^{-1}$ = 3.5/2125, 4.0/3408, 4.5/7182, 5.0/10 078, 5.5/11 405, 6.0/12 004;[52] 6.5−10.0/12 100)[53] and/or 445 nm (ε = 3600 $L{\cdot}mol^{-1}{\cdot}cm^{-1}$),[53] using a Varian Cary 50 Bio UV/vis spectrophotometer coupled to a thermostatic bath. Reactions were monitored to less than 5% conversion of 2,4-BDNPP to 2,4-DNP, and the data were treated using the initial rate method.

The activity of complexes **1** and **2** in the cleavage of 2,4-BDNPP is strongly influenced by the pH of the reaction mixture and reveals sigmoidal-shape profiles (Figure S8 in the Supporting Information). The data were fitted using a Boltzman model, resulting in pK_a = 6.36 ± 0.1 for complex **1** and pK_a = 7.45 ± 0.1 for complex **2**. In fact, the kinetic pK_a = 6.36 is in good agreement with the value found in the potentiometric titration for complex **1** (pK_a = 6.13). However, for complex **2**, the pK_a = 7.45 is around 2.0 pH units higher than that calculated from the potentiometric experiments (pK_a = 5.50). A plausible explanation for this experimental observation is based on the strong interaction of the substrate 2,4-DBNPP with catalyst **2** due to the formation of strong hydrogen bonds between the entering substrate and the protonated phenol ligand (vide infra) that in some way affects the Lewis acidity of the Cu^{II} centers, which are much more antiferromagnetically coupled in **2** compared to **1**, although such an interpretation should be considered only speculative at present because no further experimental and theorethical evidence is available at present. Therefore, deprotonation of a Cu^{II}-coordinated water molecule may occur at a higher pH to generate the catalytically active species [(OH)Cu^{II}(μ-alkoxo)-Cu^{II}(H_2O)] (species H_2C in Scheme 2) in complex **2**.

The studies on the hydrolysis rate as a function of the 2,4-BDNPP concentration in reactions catalyzed by complexes **1** and **2** were carried out at pH 8.0, where both complexes showed the highest activity in the catalysis (Figure 12). Initially, the cleavage rate increases linearly with an increase in the 2,4-BDNPP concentration, but it deviates gradually from linearity and tends toward a saturation curve at higher concentrations of the substrate. The data were treated using the Michaelis−Menten model, and the parameters V_{max}, K_M, and $k_{cat.}$ were obtained by nonlinear least-squares fits. The kinetic parameters for the hydrolysis of 2,4-BDNPP promoted by complexes **1** and **2** are described in Table 10, together with the data for **3**, where it can be observed that complex **2** is most effective in the conversion of substrate to products, with a turnover rate that is 1329 times faster than that of the uncatalyzed reaction (k_{unc} = 3.88×10^{-7} s^{-1} at pH 8.0 at 50 °C).[41]

A comparison of the kinetic parameters obtained for complexes **1** and **2** with those previously described for **3**[6] reveals that the presence of the electron-donor *tert*-butyl groups in complexes **1** and **2** caused significant changes in the hydrolytic cleavage of the substrate 2,4-BDNPP.[6] As expected, according to the pK_a values for the equilibrium [(H_2O)Cu^{II}(μ-alkoxo)Cu^{II}(H_2O)] ↔ [(OH)Cu^{II}(μ-alkoxo)Cu^{II}(H_2O)], in which the catalytically active species is generated, complex **2**, which has the highest pK_a (7.45), is the most active in the hydrolysis of the diester, while complex **3** has the lowest catalytic turnover rate because it has the lowest pK_a (6.2) and thus the lowest nucleophilic reactivity of the Cu^{II}-bound OH^- group. A similar trend has recently been observed for a series of dinuclear mixed-valence [Fe^{III}(μ-OH)Zn^{II}(L-R)] complexes in which the catalytic turnover $k_{cat.}$ for the hydrolysis of 2,4-BDNPP has a linear dependence on the pK_a values (LFER) attributed to deprotonation of the terminal Fe^{III}-bound water for distinct substituents in the ligand L-R.[52]

Concerning the affinity of the substrate 2,4-BDNPP with the catalysts **1**−**3** to generate the intermediate substrate/complex, it is observed that the reactions follow a trend similar to that observed for $k_{cat.}$, with **2** showing the highest association

dx.doi.org/10.1021/ic201876k | *Inorg. Chem.* 2012, 51, 1569−1589

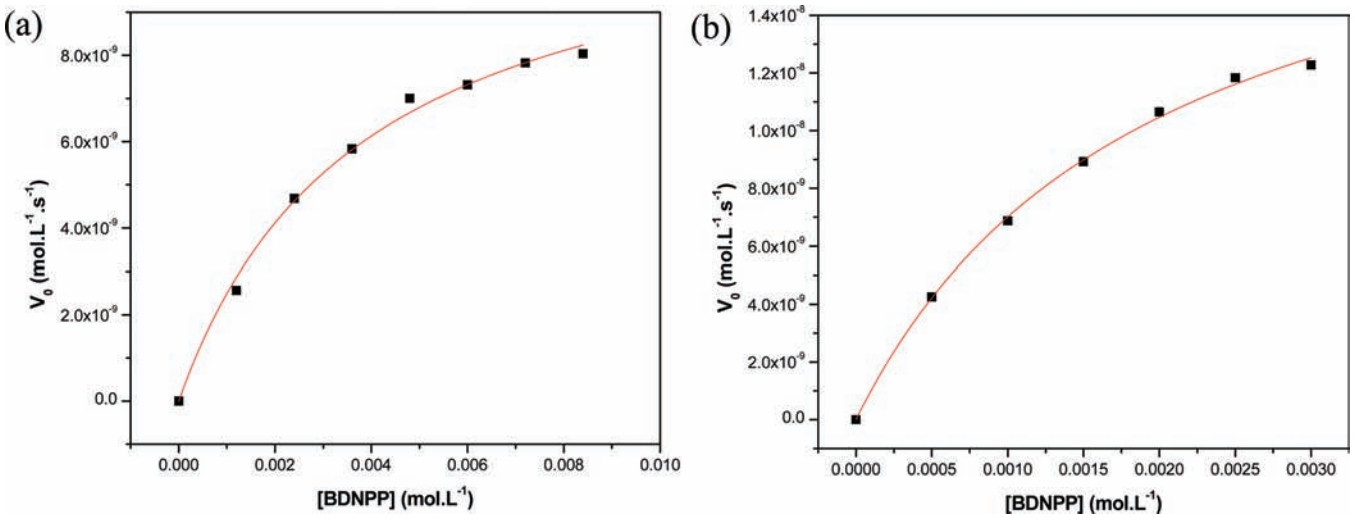

Figure 12. Dependence of the initial reaction rate on the 2,4-BDNPP concentration for the hydrolysis reaction promoted by complexes **1** (a) and **2** (b). Conditions: solution 1:1 CH_3CN/H_2O; [complex] = 4.0×10^{-5} mol·L^{-1}; [buffer] = 0.05 mol·L^{-1} HEPES (pH 8.0); I = 0.05 mol·L^{-1} $LiClO_4$; [2,4-BDNPP] = $(0.5-8.0) \times 10^{-3}$ mol·L^{-1} at 50 °C.

Table 10. Kinetic Parameters for the Hydrolysis Reaction of 2,4-BDNPP, Catalyzed by Complexes 1 and 2

complex	V_{max} (mol·L^{-1}·s^{-1})	K_M (mol·L^{-1})	$k_{cat.}$ (s^{-1})	$K_{ass.}$ (L·mol^{-1})	$k_{cat.}/K_M$	$k_{cat.}/k_{unc}$ (M^{-1}·s^{-1})
1	1.19×10^{-8}	3.82×10^{-3}	2.97×10^{-4}	261.78	0.08	767
2	2.06×10^{-8}	1.95×10^{-3}	5.16×10^{-4}	512.82	0.26	1329
3[a]	0.9×10^{-8}	9.68×10^{-3}	1.80×10^{-4}	103.30	0.02	86

[a] **3** represents the complex $[Cu_2(Hbtppnol)(OAc)]^{2+}$.[6]

constant $K_{ass.}$ and complex **3** the lowest. However, if we consider the formal charges of the complexes, the reverse behavior would be expected under identical experimental conditions. We tentatively explain these results by taking into account the possibility of strong hydrogen-bond formation between the entering substrate and the protonated phenol ligands in complexes **1** and **2** (vide supra) that should also contribute to stabilization of the transition state in these hydrolysis reactions. The pK_a = 7.45 obtained from kinetic measurements for **2** (assigned to dissociation of the Cu^{II}-bound H_2O in the substrate/complex intermediate), which is ~2.0 pH units higher than that calculated from the potentiometric experiments, strongly corroborates this assignment, and thus complex **2** shows a catalytic efficiency that is 10 times higher than that observed for complex **3**. A double electrophilic activation of the phosphodiester by coordination to the metal center and hydrogen bonding to the ammonium-functionalized ligand in a mononuclear copper(II) complex has been postulated to accelerate hydrolysis with a greater efficiency compared to related systems that do not contain such a functional group.[87] The dinuclear $Fe^{III}Mn^{II}$ sweet potato PAP has considerably higher substrate turnover rates than other PAPs, and this has been interpreted in terms of Glu365 and Asp158 acting as proton donors for the leaving groups, at least at low pH.[88]

In order to assess the possible hydrolysis of the monoester 2,4-DNPP, one of the products formed from the hydrolysis of the diester 2,4-BDNPP, stoichiometric reactions between complexes **1** and **2** and the substrate 2,4-BDNPP were monitored. It was observed that, for both complexes, over 7 days at 50 °C, only 1 equiv of 2,4-dinitrophenolate is released, which indicates only diesterase activity of **1** and **2**. Because our main goal was to obtain an effective catalyst, a hydrolysis reaction of 2,4-BDNPP (2.0×10^{-3} mol·L^{-1}) promoted by complexes **1** and **2** (4.0×10^{-5} mol·L^{-1}) at 445 nm, pH 8.0, and 50 °C was also monitored. These data revealed that over 24 h the complexes were able to hydrolyze 5 and 20 molecules of substrate for complexes **1** and **2**, respectively. Furthermore, the measured deuterium kinetic isotope effect[89] k_H/k_D of 0.89 for **1** and 0.80 for **2** suggests that no proton transfer is involved in the rate-limiting step and thus supports an intramolecular nucleophilic attack.

On the basis of the X-ray structures, solution studies, and kinetic data, the mechanism shown in Figure 13 is proposed for the hydrolysis reaction of the phosphate diester 2,4-BDNPP by complexes **1** and **2**. The dependence of the reaction rate on the pH indicates that the active species in the hydrolysis reaction is the aquo/hydroxo form of the complexes $[(OH)Cu^{II}(\mu\text{-alkoxo})\text{-}Cu^{II}(H_2O)]$, in agreement with the potentiometric titration results, which is formed when a proton is removed from one of the Cu^{II}-bound water molecules in the complexes. This species possesses a labile coordination site (H_2O) that permits the binding of a substrate molecule to a metallic center and a metal-coordinated nucleophile group (OH^-) available for intramolecular attack. We propose double electrophilic activation of the phosphodiester by monodentate coordination to the Cu^{II} center that contains the phenol group with *tert*-butyl substituents and hydrogen bonding of the protonated phenol with the phosphate O atom. This increases the $K_{ass.}$ and $k_{cat.}$ values in comparison with those found for complex **3**.[6] In the next step, an intramolecular nucleophilic attack by the cis-oriented $Cu^{II}OH$ group leads to the release of 2,4-dinitrophenolate and bridging coordination of the monoester 2,4-DNPP. Finally, the μ-1,3-coordinated monoester intermediate undergoes substitution by two water molecules and regenerates the active site for the next catalytic cycle. Under stoichiometric conditions, the release of

dx.doi.org/10.1021/ic201876k | *Inorg. Chem.* 2012, 51, 1569–1589

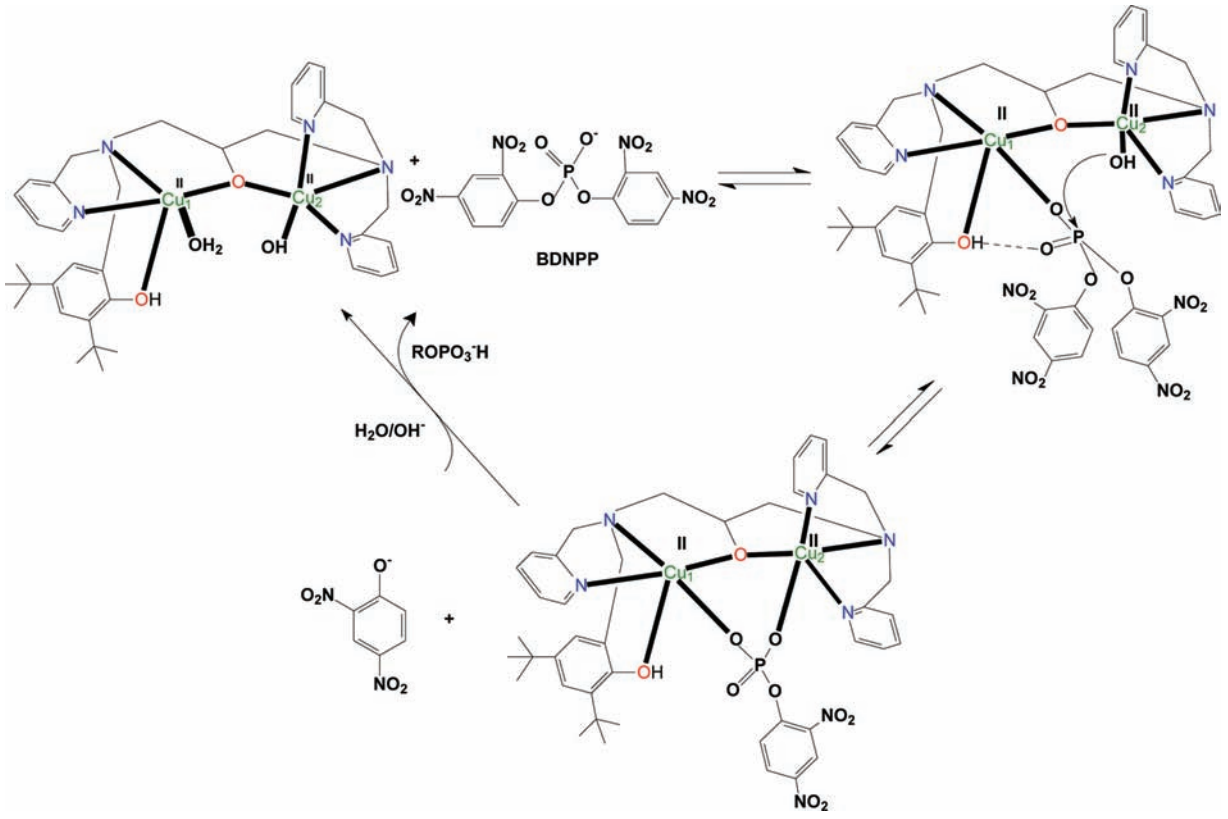

Figure 13. Proposed mechanism for hydrolysis of 2,4-BDNPP catalyzed by complex **1**. The mechanism proposed for **2** is similar.

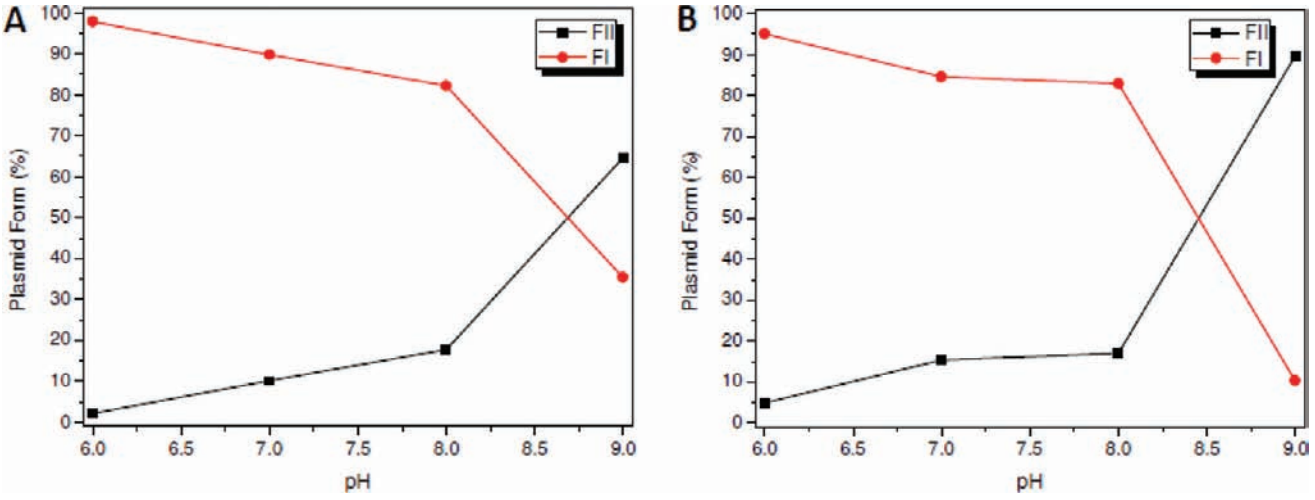

Figure 14. Plot of % plasmid DNA forms (FI and FII) after incubation with a concentration of 20 μM **1** (A) and **2** (B) at different pH values for 6 h at 37 °C. Different buffers (25 mmol·L^{-1}) were used according to the pH: PIPES (pH 6.0 and 7.0), HEPES (pH 8.0), and CHES (pH 9.0).

only 1 equiv of 2,4-dinitrophenolate was observed, which suggests the formation of a stable Cu(μ-2,4-DNPP)Cu complex.

DNA Cleavage Activity. Complexes **1** and **2** were assayed in the cleavage of plasmid DNA (pBSK II, 30 μmol·L^{-1} bp) to assess their nuclease activity. DNA cleavage was measured by the conversion of supercoiled DNA (FI) to the open-circular (FII) and/or linear (FIII) forms. Free Cu ions were not observed to cleave supercoiled DNA under the conditions of this study (6 h of incubation at 37 °C; Figure S9 in the Supporting Information).

Initially, the DNA cleavage activity of **1** and **2** was analyzed within a broad pH range (6.0–9.0). Figure 14 presents a pH-dependent profile for DNA cleavage promoted by both complexes (20 μmol·L^{-1}) at 37 °C, which indicates that the cleavage rate increases with an increase in the pH value, with maximum activity at pH 9.0.

The effect of the complex concentration on the cleavage of DNA was investigated under the optimum pH conditions. Figure 15 shows that both complexes were able to cleave DNA at all concentrations assayed (10–50 μmol·L^{-1}). The amount of cleaved DNA increased with an increase in the concentration of the complexes. After 6 h of incubation at 37 °C, a 50 μmol·L^{-1} solution of **1** and **2** converted ~70% and 84%, respectively, of supercoiled DNA (FI) to open-circular DNA (FII). Complex **2** also promoted the formation of 15.3% linear DNA (FIII).

dx.doi.org/10.1021/ic201876k | Inorg. Chem. 2012, 51, 1569–1589

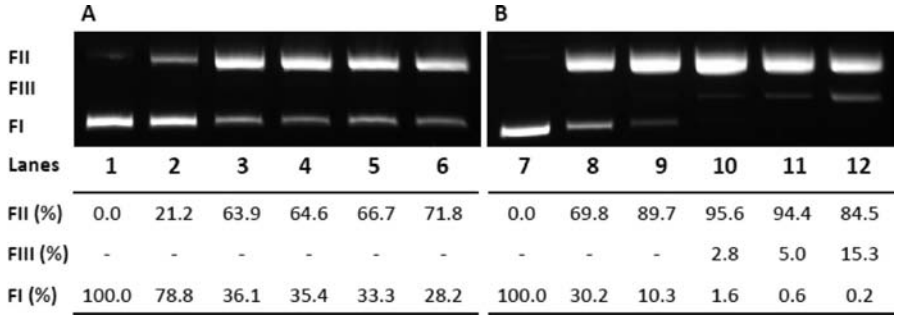

Lanes	1	2	3	4	5	6	7	8	9	10	11	12
FII (%)	0.0	21.2	63.9	64.6	66.7	71.8	0.0	69.8	89.7	95.6	94.4	84.5
FIII (%)	-	-	-	-	-	-	-	-	-	2.8	5.0	15.3
FI (%)	100.0	78.8	36.1	35.4	33.3	28.2	100.0	30.2	10.3	1.6	0.6	0.2

Figure 15. Agarose gel electrophoresis of plasmid DNA cleavage by **1** (A) and **2** (B) at different concentrations and at optimum pH [25 mmol·L^{-1} CHES (pH 9.0)]. Lanes 1 and 7: DNA control. Lanes 2–6: DNA + **1** (10, 20, 30, 40, and 50 μmol·L^{-1}, respectively). Lanes 8–12: DNA + **2** (10, 20, 30, 40, and 50 μmol·L^{-1}, respectively). Incubation: 6 h at 37 °C.

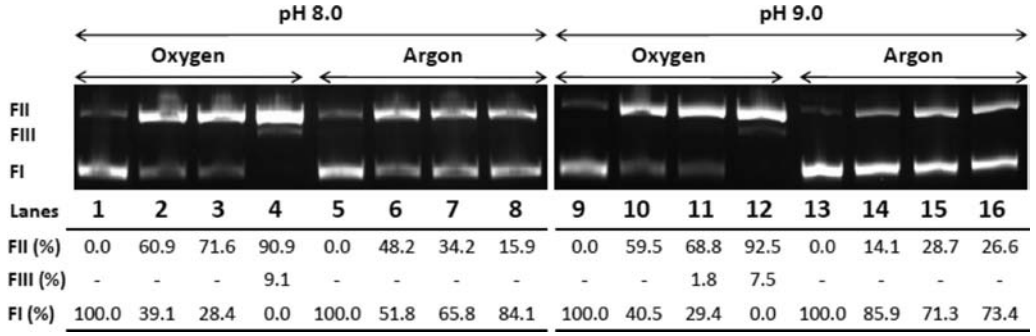

Lanes	1	2	3	4	5	6	7	8	9	10	11	12	13	14	15	16
FII (%)	0.0	60.9	71.6	90.9	0.0	48.2	34.2	15.9	0.0	59.5	68.8	92.5	0.0	14.1	28.7	26.6
FIII (%)	-	-	-	9.1	-	-	-	-	-	-	1.8	7.5	-	-	-	-
FI (%)	100.0	39.1	28.4	0.0	100.0	51.8	65.8	84.1	100.0	40.5	29.4	0.0	100.0	85.9	71.3	73.4

Figure 16. Cleavage of pBSK II (25 μmol·L^{-1} bp) by complex **1** under aerobic (oxygen atmosphere) and anaerobic (argon atmosphere) conditions at pH 8.0 (25 mmol·L^{-1} HEPES buffer) and 9.0 (25 mmol·L^{-1} CHES buffer). Lanes 1, 5, 9, and 13: DNA control. Lanes 2 and 6: DNA + **1** (40 μmol·L^{-1}). Lanes 3 and 7: DNA + **1** (100 μmol·L^{-1}). Lanes 10 and 14: DNA + **1** (20 μmol·L^{-1}). Lanes 11 and 15: DNA + **1** (40 μmol·L^{-1}). Lanes 4, 8, 12, and 16: 100 μM Fe-EDTA + 10 mmol·L^{-1} DTT. Incubation: 6 h at 37 °C.

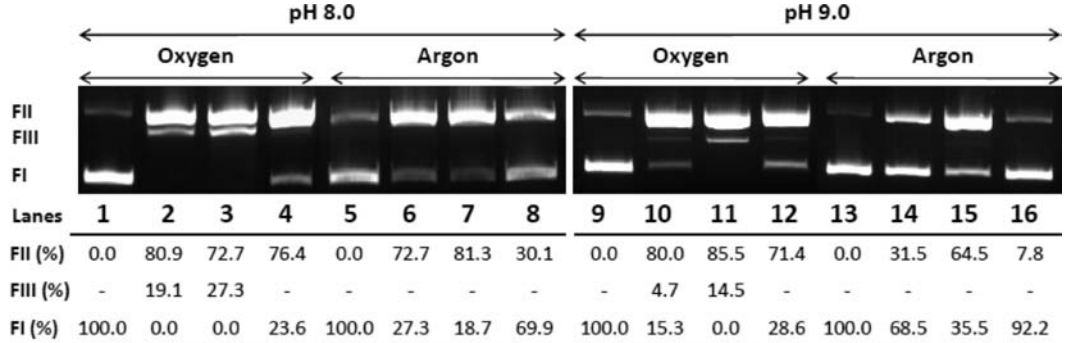

Lanes	1	2	3	4	5	6	7	8	9	10	11	12	13	14	15	16
FII (%)	0.0	80.9	72.7	76.4	0.0	72.7	81.3	30.1	0.0	80.0	85.5	71.4	0.0	31.5	64.5	7.8
FIII (%)	-	19.1	27.3	-	-	-	-	-	-	4.7	14.5	-	-	-	-	-
FI (%)	100.0	0.0	0.0	23.6	100.0	27.3	18.7	69.9	100.0	15.3	0.0	28.6	100.0	68.5	35.5	92.2

Figure 17. Cleavage of pBSK II (25 μmol·L^{-1} bp) by complex **2** under aerobic (oxygen atmosphere) and anaerobic (argon atmosphere) conditions at pH 8.0 (25 mmol·L^{-1} HEPES buffer) and 9.0 (25 mmol·L^{-1} CHES buffer). Lanes 1, 5, 9, and 13: DNA control. Lanes 2 and 6: DNA + **2** (30 μmol·L^{-1}). Lanes 3 and 7: DNA + **2** (40 μmol·L^{-1}). Lanes 10 and 14: DNA + **2** (10 μmol·L^{-1}). Lanes 11 and 15: DNA + **2** (20 μmol·L^{-1}). Lanes 4, 8, 12, and 16: 100 μmol·L^{-1} Fe-EDTA + 10 mmol·L^{-1} DTT. Incubation: 6 h at 37 °C.

In order to determine the influence of O_2 on the DNA cleavage process, an aerobic versus anaerobic (argon atmosphere) experiment was performed at pH 8.0 and 9.0. It was observed that DNA cleavage promoted by **1** was inhibited in an argon atmosphere at both pH values (Figure 16). However, the inhibition was substantially greater at pH 9.0 than pH 8.0, indicating a major oxidative mechanism at pH 9.0 and a major hydrolytic mechanism at pH 8.0. According to the potentiometric titration species distribution curves (see the Potentiometric Titration section), at pH 8.0, there is a higher percentage of the aquo/hydroxo form of the complex [(OH)Cu^{II}(μ-alkoxo)-Cu^{II}(H_2O)]. Thus, this species is most probably associated with the hydrolysis of plasmid DNA, as was observed in catalysis of the model substrate 2,4-BDNPP. Consequently, at pH 9.0, the hydrolytic activity of **1** declines because the percentage of aquo/hydroxo species decreases considerably, but this is the optimum pH, probably because of the fact that the oxidative activity increases. Concerning complex **2**, a similar behavior was observed in an argon atmosphere because the nuclease activity also showed a greater decrease at pH 9.0 than at pH 8.0, suggesting a higher hydrolytic activity at pH 8.0, where the aquo/hydroxo form of the complex is also the active species in catalysis. However, at pH 9.0, the inhibition was only partial, indicating a mixed cleavage mechanism involving hydrolysis and oxidation of plasmid DNA in similar proportions (see Figure 17). Thus, at the optimum pH, the oxidative activity is higher for complex **1**, as observed in oxidation

dx.doi.org/10.1021/ic201876k | Inorg. Chem. 2012, 51, 1569–1589

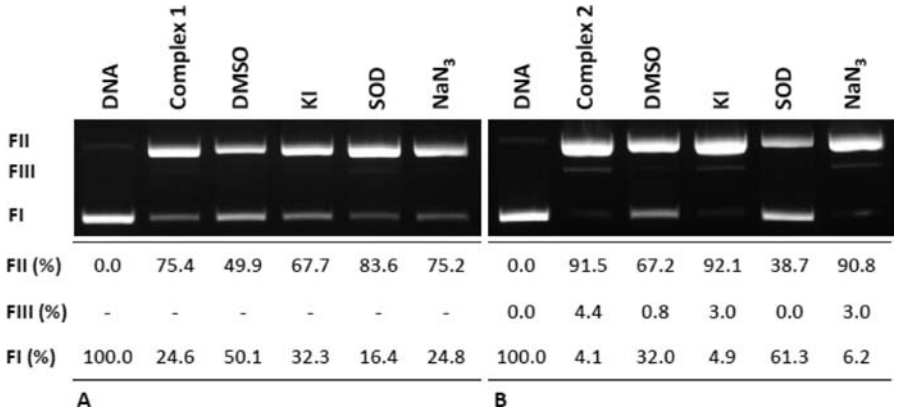

Figure 18. DNA cleavage of plasmid DNA pBSK II (25 μmol·L^{-1} in bp) by **1** (40 μmol·L^{-1}) (A) and **2** (10 μmol·L^{-1}) (B) for 6 h at 37 °C with different cleavage inhibitors: DMSO (10% v/v), KI (500 μmol·L^{-1}), SOD (20 units), and NaN_3 (500 μmol·L^{-1}).

of the model substrate 3,5-DTBC, and the hydrolytic activity is more pronounced for complex **2**, as obtained in hydrolysis of the model substrate 2,4-BDNPP (see the Reactivity section).

In addition, the ROS involved in the oxidative DNA cleavage process was investigated by the use of different potential inhibitors (see Figure 18). The DNA cleavage promoted by **1** was inhibited in the presence of DMSO and KI, which suggests that hydroxyl radicals and hydrogen peroxide play an important role in the cleavage mechanism pathway (Figure 20A). In contrast, the nuclease activity of **2** was attenuated in the presence of DMSO and SOD, indicating participation of the hydroxyl and superoxide radicals in the scission event (Figure 20B). Furthermore, in the presence of the copper(I) chelator bathocuproine, the activity of **1** and **2** was significantly reduced (Figure 19), demonstrating that the reduction of Cu^{II} to Cu^{I} is an important step in the cleavage process.

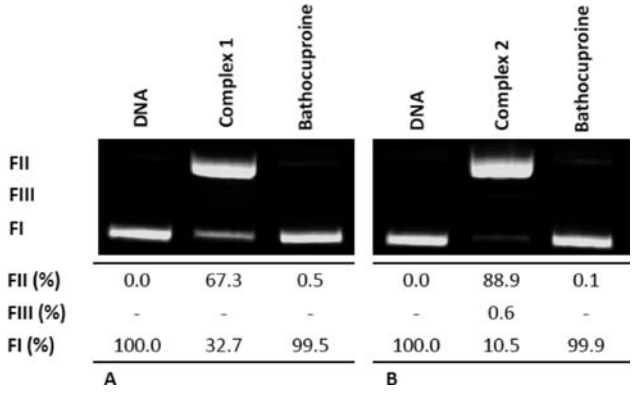

Figure 19. Effect of bathocuproine (500 μmol·L^{-1}) on the plasmid DNA cleavage by **1** (40 μmol·L^{-1}) (A) and **2** (10 μmol·L^{-1}) (B). Reactions were performed in 25 mmol·L^{-1} CHES (pH 9.0) and incubated for 6 h at 37 °C.

Moreover, to study the binding of the complexes to DNA, assays were performed using the minor groove binder distamycin and the major groove binder methyl green. Figure 20A shows the results obtained with **1**. No apparent inhibition of the DNA cleavage activity was observed, indicating that interaction of this complex with plasmid DNA does not occur through the grooves. However, the DNA damage produced by **2** was partially inhibited in the presence of distamycin (see Figure 20B). This finding indicates that complex **2** interacts through the minor groove and then cleaves the plasmid DNA.

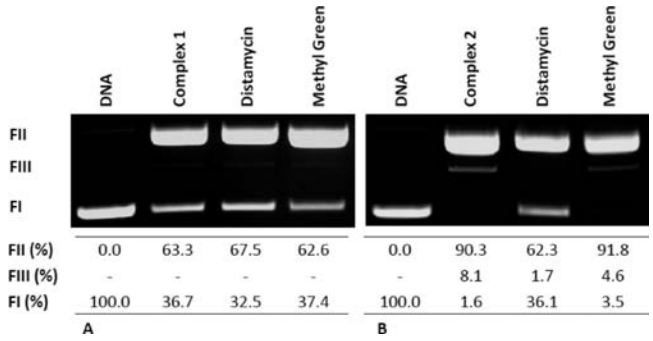

Figure 20. Influence of DNA groove binders distamycin and methyl green (50 μmol·L^{-1}) on the DNA cleavage activity of **1** (40 μmol·L^{-1}) (A) and **2** (10 μmol·L^{-1}) (B). Reactions were performed in 25 mmol·L^{-1} CHES (pH 9.0) and incubated for 6 h at 37 °C.

The effect of the ionic strength on the nuclease activity of both complexes was determined by observing the effect of NaCl on the DNA cleavage reaction. Figure 21 shows that the process of cleavage by both complexes was sensitive to a change in the ionic strength. The extent of DNA cleavage decreased from more than 90% to a maximum of 30% and 50% for **1** and **2**, respectively, when the ionic strength increased from 20 to 200 mmol·L^{-1}. These results suggest that electrostatic interactions contribute to the DNA cleavage because the DNA molecule is negatively charged and complexes **1** and **2** present a positive net charge.

These results led us to propose a mechanistic pathway through which the complexes cleave the plasmid DNA at optimum pH. Complex **1** approaches plasmid DNA via electrostatic interactions with the phosphate backbone of DNA, and the Cu^{II} sites are reduced to Cu^{I}. This reduction can be attributed to electron transfer between the complex and DNA in solution.[90] O_2 then reacts with the copper(I) complex, generating $OH^{\bullet}$, which attacks the DNA. Complex **2**, in contrast, interacts with DNA via electrostatic attraction and binds to the minor groove. The oxidative cleavage occurs as described for complex **1**, but the radicals $OH^{\bullet}$ and O_2^{-} are generated as ROS. In a second pathway, the binding of the aquo/hydroxo form of the complex at the minor groove promotes the hydrolysis of DNA.

Kinetic measurements were carried out to monitor the decrease in the amount of supercoiled DNA at different reaction times and complex concentrations. The plots of k_{obs} values versus concentrations of both complexes are shown in

dx.doi.org/10.1021/ic201876k | Inorg. Chem. 2012, 51, 1569–1589

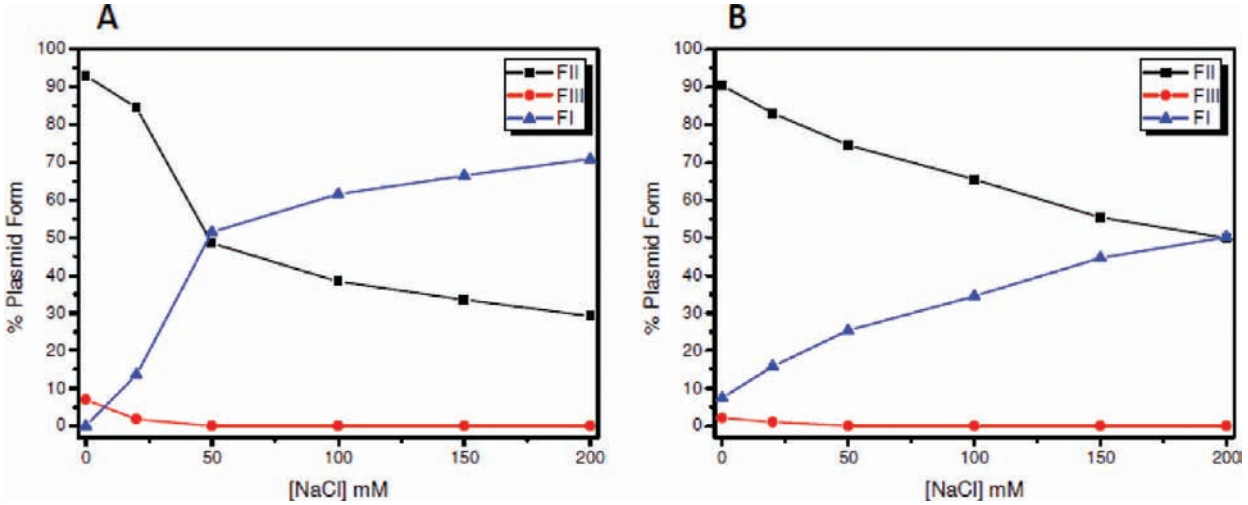

Figure 21. Effect of the ionic strength on supercoiled plasmid DNA cleavage by **1** (80 μmol·L^{-1}) (A) and **2** (10 μmol·L^{-1}) (B). Reaction conditions: 25 mmol.L^{-1} CHES buffer (pH 9.0). Incubation: 6 h at 37 °C.

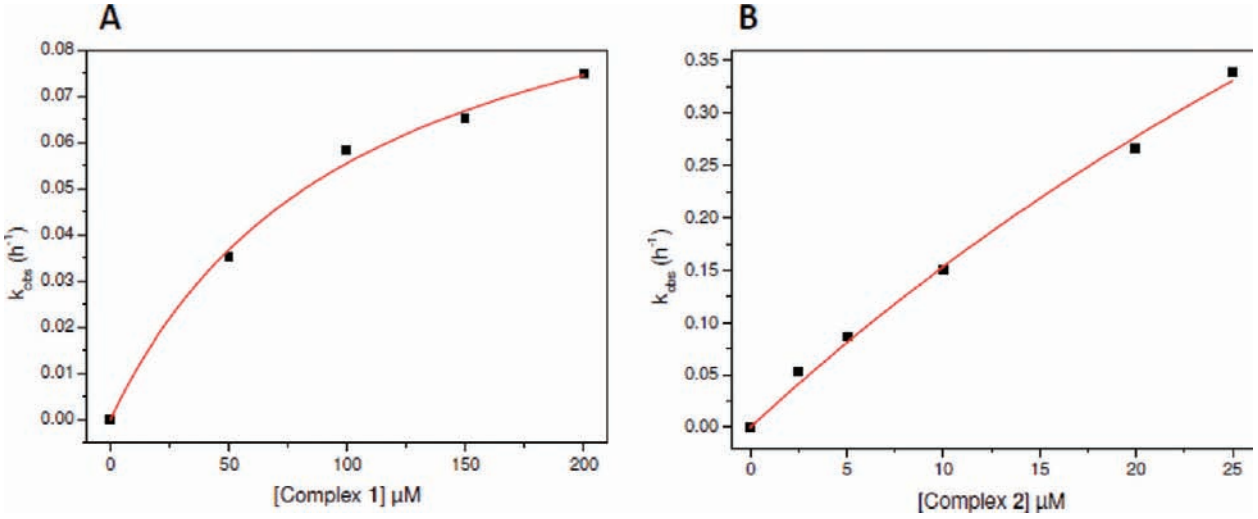

Figure 22. Plot of k_{obs} values versus concentrations of complexes **1** (A) and **2** (B), showing saturation behavior. Reactions were performed at pH 9.0 (25 mmol·L^{-1} CHES buffer) with 300 ng (25 μmol·L^{-1} bp) of plasmid pBSK II and different concentrations of the complexes. Incubations were performed at 37 °C, and aliquots were removed at different time intervals (0−6 h).

Figure 22. The pseudo-Michaelis−Menten kinetic parameters are listed in Table 11.

Table 11. Kinetic Parameters of 1 and 2 in DNA Cleavage under Pseudo-Michaelis−Menten Conditions

complex	$k_{cat.}$[a] (h^{-1})	K_M (mol·L^{-1})	$k_{cat.}/K_M$[b] (h^{-1}·mol^{-1}·L)	$k_{cat.}/k_{unc}$[c]	$t_{1/2}$[d] (h)
1	0.12	1.2×10^{-4}	1.0×10^{3}	3.4×10^{6}	5.8
2	0.55	2.4×10^{-5}	2.3×10^{4}	1.5×10^{7}	1.3

[a]Catalytic constant (i.e., V_{max} at the saturation level). [b]Catalytic efficiency. [c]Rate enhancement compared to uncatalyzed cleavage of double-stranded DNA ($k_{unc} = 3.6 \times 10^{-8}$ h^{-1}). [d]Supercoiled DNA half-life time ($t_{1/2} = -\ln(0.5)/k_{cat.}$).

As is well-known, the first-order hydrolysis rate constant for a phosphodiester bond of double-stranded DNA is estimated to be 3.6×10^{-8} h^{-1}. Reported rate enhancements for copper(II) complexes are in the range of 1.1×10^{6}−2.3×10^{8}-fold.[55,90] The $k_{cat.}$ values of 0.12 and 0.55 h^{-1} obtained for **1** and **2**, respectively, indicate that these complexes exhibit high cleavage reactivity, with 3.4×10^{6}- and 1.5×10^{7}-fold rate enhancements, respectively. Compared to the previously published complex **3** (k_{obs} = 0.022 h^{-1}; half-life = 30.91 h, rate enhancement of DNA cleavage of 6.2×10^{5} at 50 °C), we clearly observe that **1** and **2** are more efficient, even at the lower temperature used in this study.

The catalytic efficiency reveals that **2** (2.3×10^{4} h^{-1}·M^{-1}) is ∼23 times more active as a chemical nuclease than **1** (1.0×10^{3} h^{-1}·M^{-1}) and the estimated supercoiled DNA half-life times in the presence of **1** and **2** are ∼5.8 and ∼1.3 h, respectively. The higher activity of complex **2** compared to complex **1** is probably due to the fact that **2** interacts more strongly with DNA (through electrostatic attractions and binding at the minor grooves) and can thus promote oxidation and hydrolysis in greater proportions.

In summary, as observed in hydrolysis of the model substrate 2,4-BDNPP, the presence of electron donor *tert*-butyl groups localized in positions ortho and para to the phenolic donor O atom in **1** and **2** caused significant changes in the plasmid DNA cleavage compared to other analogous dinuclear copper(II) complexes found in the

dx.doi.org/10.1021/ic201876k | *Inorg. Chem.* 2012, 51, 1569−1589

literature,[6,91,92] because of stronger interaction of the catalysts **1** and **2** with the phosphate diester backbone.

CONCLUSIONS

In summary, we have synthesized and fully characterized two unsymmetrical dinuclear $[Cu^{II}(\mu\text{-alkoxo})(\mu\text{-carboxylato})Cu^{II})]$ complexes **1** and **2**, in which the Cu^{II} centers have distinct coordination environments: while the Cu1 centers have square-pyramidal geometry and are bound to the hard sites of the **L1** and **L2** ligands, the Cu2 centers show a distorted square-pyramidal arrangement and are coordinated to the tridentate soft sites of the ligands. Complex **3** was referred to in the discussion of the results for comparison purposes. Magnetic susceptibility revealed that the Cu^{II} centers in **1** and **2** are antiferromagnetically coupled and that the difference in the exchange coupling J found for these complexes ($J = -4.3$ cm^{-1} for **1** and $J = -40.0$ cm^{-1} for **2**) is a function of the Cu−O−Cu bridging angle, in good agreement with DFT/BS theoretical calculations. We proposed that the greater bridging Cu−O−Cu angle (θ) of 130.66° in **2** compared to 124.7° in complex **1** could lead to some mixing of the d_{z^2} orbital associated with the trigonal-bipyramidal geometry with the $d_{x^2-y^2}$ ground state of the square pyramid, thus giving rise to stronger antiferromagnetism ($J = -40$ cm^{-1}) in **2**. Kinetic studies revealed that **1** and **2** are efficient catalysts in the oxidation of 3,5-di-*tert*-butylcatechol by O_2, with complex **2** being the most active because it is the strongest oxidant compared to **1** and **3**. In addition, the complexes were shown to efficiently catalyze hydrolysis of the diester model substrate 2,4-bis-(dinitrophenyl)phosphate and to cleave plasmid DNA under mild pH and temperature conditions in the following order of reactivity: **2** > **1** > **3**. Herein, we proposed that double electrophilic activation of the phosphodiester 2,4-BDNPP by monodentate coordination to the Cu^{II} center that contains the phenol group with *tert*-butyl substituents and hydrogen bonding of the protonated phenol with the phosphate O atom increase the hydrolase activity ($K_{ass.}$ and $k_{cat.}$) of **1** and **2** in comparison with that found for complex **3**.

ASSOCIATED CONTENT

Supporting Information

X-ray crystallographic data in CIF format and Figures S1−S9. This material is available free of charge via the Internet at http://pubs.acs.org. Crystallographic data (without structure factors) for the structure(s) reported in this paper have also been deposited with the Cambridge Crystallographic Data Centre as CCDC 802096 for complex **1** and CCDC 802100 for complex **2**. Copies of the data can be obtained free of charge from the CCDC (12 Union Road, Cambridge CB2 1EZ, U.K.; tel (+44) 1223-336-408; fax (+44) 1223-336-003; e-mail deposit@ccdc.cam.ac.uk; web site www.ccdc.cam.ac.uk).

AUTHOR INFORMATION

Corresponding Author

*E-mail: ademir@qmc.ufsc.br. Tel.: +55 4837219219. Fax: +55 4837219711.

ACKNOWLEDGMENTS

The authors are grateful for grants awarded to support this research from CNPq, FAPESC, CAPES-PROCAD, and INCT-Catálise (Brazil), BMBF/IB (Germany), and NN202103238 (Poland). We thank Juraj Pelikan for some magnetic experiments.

REFERENCES

(1) Than, R.; Feldmann, A. A.; Krebs, B. *Coord. Chem. Rev.* **1999**, *182*, 211−241.
(2) Mitić, N.; Smith, S. J.; Neves, A.; Guddat, L. W.; Gahan, L. R.; Schenk, G. *Chem. Rev.* **2006**, *106*, 3338−3363.
(3) Gahan, L. R.; Smith, S.; Neves, A.; Schenk, G. *Eur. J. Inorg. Chem.* **2009**, 2745−2758.
(4) Greatti, A.; Scarpellini, M.; Peralta, R. A.; Casellato, A.; Bortoluzzi, A. J.; Xavier, F. R.; Jovito, R.; de Brito, M. A.; Szpoganicz, B.; Tomcowicz, Z.; Rams, M.; Haase, W.; Neves, A. *Inorg. Chem.* **2008**, *47*, 1107−1119.
(5) Neves, A.; Lanznaster, M.; Bortoluzzi, A.; Peralta, R. A.; Casellato, A.; Castellano, E. E.; Herrald, P.; Riley, M. J.; Schenk, G. *J. Am. Chem. Soc.* **2007**, *129*, 7486−7487.
(6) Rossi, L. M.; Neves, A.; Bortoluzzi, A. J.; Hörner, R.; Szpoganicz, B.; Terenzi, H.; Mangrich, A. S.; Pereira-Maia, E. C.; Castellano, E.; Haase, W. *Inorg. Chim. Acta* **2005**, *358*, 1807−1822.
(7) Liu, C.; Zhou, J.; Li, Q.; Wang, L.; Liao, Z.; Xu, H. *J. Inorg. Biochem.* **1999**, *75*, 233−240.
(8) Neves, A.; Rossi, L. M.; Horn, A. Jr.; Vencato, I.; Bortoluzzi, A. J.; Zucco, C.; Mangrich, A. S. *Inorg. Chem. Commun.* **1999**, *2*, 334−337.
(9) Itoh, T.; Hisada, H.; Usui, Y.; Fujii, Y. *Inorg. Chim. Acta* **1998**, *283*, 51−60.
(10) Young, M. J.; Wahnon, D.; Hynes, R. C.; Chin, J. *J. Am. Chem. Soc.* **1995**, *117*, 9441−9447.
(11) De Rosch, M. A.; Trogler, W. C. *Inorg. Chem.* **1990**, *29*, 2409−2416.
(12) Hendry, P.; Sargeson, A. M. *J. Am. Chem. Soc.* **1989**, *111*, 2521−2527.
(13) Morrow, J. R.; Trogler, W. C. *Inorg. Chem.* **1988**, *27*, 3387−3394.
(14) Gichinga, M. G.; Striegler, S. *J. Am. Chem. Soc.* **2008**, *130*, 5150−5156.
(15) Rey, N. A.; Neves, A.; Bortoluzzi, A. J.; Pich, C. T.; Terenzi, H. *Inorg. Chem.* **2007**, *46*, 348−350.
(16) Weng, C. H.; Cheng, S. C.; Wei, H. M.; Wei, H. H.; Lee, C. J. *Inorg. Chim. Acta* **2006**, *359*, 2029−2040.
(17) Peralta, R. A.; Neves, A.; Bortoluzzi, A. J.; dos Anjos, A.; Xavier, F. R.; Szpoganicz, B.; Terenzi, H.; de Oliveira, M. C. B.; Castellano, E. E.; Friedermann, G. R.; Mangrich, A. S.; Novak, M. A. *J. Inorg. Biochem.* **2006**, *100*, 992−1004.
(18) Selmeczi, K.; Réglier, M.; Giorgi, M.; Speier, G. *Coord. Chem. Rev.* **2003**, *245*, 191−201.
(19) Torelli, S.; Belle, C.; Hamman, S.; Hamman, S.; Pierre, J.-L. *Inorg. Chem.* **2002**, *41*, 3983−3989.
(20) Belle, C.; Beguin, C.; Gautier-Luneau, I.; Hamman, S.; Philouze, C.; Pierre, J.-L.; Thomas, F.; Torelli, S. *Inorg. Chem.* **2002**, *41*, 479−491.
(21) Kaizer, J.; Pap, J.; Speier, G.; Párkányi, L.; Korecz, L.; Rockenbauer, A. *J. Inorg. Biochem.* **2002**, *91*, 190−198.
(22) Neves, A.; Rossi, L. M.; Bortoluzzi, A. J.; Szpoganicz, B.; Wiezbicki, C.; Schwingel, E. *Inorg. Chem.* **2002**, *41*, 1788−1794.
(23) Neves, A.; Rossi, L. M.; Bortoluzzi, A. J.; Mangrich, A. S.; Haase, W.; Werner, R. *J. Braz. Chem. Soc.* **2001**, *12*, 747−754.
(24) Manzur, J.; Garcia, A. M.; Córdova, C.; Pizarro, O.; Acuña, V.; Spodine, E. *Polyhedron* **2002**, *21*, 181−185.
(25) Wegner, R.; Dubs, M.; Görls, H.; Robl, C.; Schönecker, B.; Jäger, E. G. *Steroids* **2002**, *67*, 835−849.
(26) Mukherjee, J.; Mukherjee, R. *Inorg. Chim. Acta* **2002**, *337*, 429−438.
(27) Gentschev, P.; Lüken, M.; Möller, N.; Rompel, A.; Krebs, B. *Inorg. Chem. Commun.* **2001**, *4*, 753−756.
(28) Fernandes, C.; Neves, A.; Bortoluzzi, A. J.; Mangrich, A. S.; Rentschler, E.; Szpoganicz, B.; Schwingel, E. *Inorg. Chim. Acta* **2001**, *320*, 12−21.
(29) Torelli, S.; Belle, C.; Gautier-Luneau, I.; Pierre, J.-L.; Saint-Aman, E.; Latour, J. M.; Le Pape, L.; Luneau, D. *Inorg. Chem.* **2000**, *39*, 3526−3536.

(30) Monzani, E.; Battaini, G.; Perotti, A.; Casella, L.; Gullotti, M.; Santagostini, L.; Nardin, G.; Randaccio, L.; Geremia, S.; Zanello, P.; Opromolla, G. *Inorg. Chem.* **1999**, *38*, 5359−5369.
(31) Oishi, N.; Nishida, Y.; Ida, K.; Kida, S. *Bull. Chem. Soc. Jpn.* **1980**, *53*, 2847−2850.
(32) Meyer, F.; Ackermann, J.; Kaifer, E.; Pritzkow, H. *Chem.—Eur. J.* **2002**, *8*, 247−258.
(33) Klabunde, T.; Eicken, C.; Sacchettini, J. C.; Krebs, B. *Nat. Struct. Biol.* **1998**, *5*, 1084−1090.
(34) Eicken, C.; Krebs, B.; Sacchettini, J. C. *Curr. Opin. Struct. Biol.* **1999**, *9*, 677−683.
(35) Eicken, C.; Zippel, F.; Büldt-Karentzpoulos, K.; Krebs, B. *FEBS Lett.* **1998**, *436*, 293−299.
(36) Gerdemann, C.; Eicken, C.; Krebs, B. *Acc. Chem. Res.* **2002**, *35*, 183−191.
(37) Scarpellini, M.; Neves, A.; Hörner, R.; Bortoluzzi, A. J.; Szpoganicz, B.; Zucco, C.; Silva, R. A. N.; Drago, V.; Mangrich, A. S.; Ortiz, W. A.; Passos, W. A. C.; De Oliveira, M. C. B.; Terenzi, H. *Inorg. Chem.* **2003**, *42*, 8353−8365.
(38) Oliveira, I. R. W. Z.; Osório, R. E. H. M. B.; Neves, A.; Vieira, I. C. *Sens. Actuators B* **2007**, *122*, 89−94.
(39) Fernandes, S. C.; Osório, R. E. H. M. B.; Anjos, A.; Neves, A.; Micke, G. A.; Vieira, I. C. *J. Braz. Chem. Soc.* **2008**, *19*, 1215−1223.
(40) Sokolowski, A.; Müller, J.; Weyhermüller, T.; Schnepf, R.; Hildebrandt, P.; Bothe, E.; Wieghardt, K. *J. Am. Chem. Soc.* **1997**, *119*, 8889−8900.
(41) Bunton, C. A.; Farber, S. J. *J. Org. Chem.* **1969**, *34* (4), 767−772.
(42) Rawji, G.; Milburn, R. M. *J. Org. Chem.* **1981**, *46*, 1205−1206.
(43) Ausubel, F. M.; Brent, R.; Kingston, R. E.; Moore, D. D.; Seidman, J. G.; Smith, J. A.; Struhl, K. *Short Protocols in Molecular Biology: A Compendium of Methods from Current Protocols in Molecular Biology*; Wiley: New York, 1999.
(44) *HiSpeed Plasmid Purification Handbook*. QIAGEN; November, 2005 (www.qiagen.com).
(45) Gagné, R. R.; Koval, C. A.; Lisensky, G. C. *Inorg. Chem.* **1980**, *19*, 2855−2857.
(46) O'Connor, C. J. *Prog. Inorg. Chem.* **1982**, *29*, 203−283.
(47) Perdew, J. P.; Wang, Y. *Phys. Rev. B* **1986**, *33*, 8800.
(48) Becke, A. D. *J. Chem. Phys.* **1993**, *98*, 5648−5652.
(49) Weigend, F.; Ahlrichs, R. *Phys. Chem. Chem. Phys.* **2005**, *7*, 3297−3305.
(50) Dunning, T. H. Jr. *J. Chem. Phys.* **1970**, *53*, 2823−2833.
(51) Martell, A. E.; Motekaitis, R. J. *Determination and Use of Stability Constants*, 2nd ed.; VHC Publishers, Inc.: Weinheim, Germany, 1992.
(52) Peralta, R. A.; Bortoluzzi, A. J.; de Souza, B.; Jovito, R.; Xavier, F. R.; Couto, R. A. A.; Casellato, A.; Nome, F.; Dick, A.; Gahan, L. R.; Schenk, G.; Hanson, G. R.; de Paula, F. C. S.; Pereira-Maia, E. C.; Machado, S. P.; Severino, P. C.; Pich, C.; Bortolotto, T.; Terenzi, H.; Castellano, E. E.; Neves, A.; Riley, M. J. *Inorg. Chem.* **2010**, *49*, 11421−11438.
(53) Batista, S. C.; Neves, A.; Bortoluzzi, A. J.; Vencato, I.; Peralta, R. A.; Szpoganicz, B.; Aires, V. V. E.; Terenzi, H.; Severino, P. C. *Inorg. Chem. Commun.* **2003**, *6*, 1161.
(54) Jin, Y.; Cowan, J. A. *J. Am. Chem. Soc.* **2005**, *127*, 8408−8415.
(55) Sreedhara, A.; Freed, J. D.; Cowan, J. A. *J. Am. Chem. Soc.* **2000**, *122*, 8814−8824.
(56) SIR97: a newtoolfor crystal structure determination and refinement: Altomare, A.; Burla, M. C.; Camalli, M.; Cascarano, G. L.; Giacovazzo, C.; Guagliardi, A.; Moliterni, A. G. G.; Polidori, G.; Spagna, R. *J. Appl. Crystallogr.* **1999**, *32*, 115−119.
(57) Sheldrick, G. M. *SHELXL-97: Program for the Refinement of Crystal Structures*; University of Göttingen: Göttingen, Germany, 1997.
(58) Spek, A. L. *Acta Crystallogr., Sect. A* **1990**, *46*, C34.
(59) Addison, A. W.; Rao, T. N. *J. Chem. Soc., Dalton Trans.* **1984**, *7*, 1349−1356.
(60) Neves, A.; Rossi, L. M.; Vencato, I.; Drago, V.; Haase, W.; Werner, R. *Inorg. Chim. Acta* **1998**, *281*, 111−115.
(61) Bill, E.; Muller, J.; Weyhermuller, T.; Wieghardt, K. *Inorg. Chem.* **1999**, *38*, 5795−5802.
(62) Adams, H.; Bailey, N. A.; Fenton, D. E. *J. Chem. Soc., Dalton Trans.* **1996**, 2233−2237.
(63) Sokolowski, A.; Leutbecher, H.; Weyhermuller, T.; Schnepf, R.; Bothe, E.; Bill, E.; Hildebrandt, P.; Wieghardt, K. *J. Biol. Inorg. Chem.* **1997**, *2*, 444−453.
(64) Wang, Y.; Dubois, J. L.; Stack, T. D. P. *Science* **1998**, *279*, 537−540.
(65) Bleaney, B.; Bowers, K. D. *Proc. R. Soc. London, Ser. A* **1952**, *214*, 451.
(66) Yi-Chian, C.; Huang, S.-F.; Koner, R.; Lee, G.-H.; Wang, Y.; Mohanta, S.; Wei, H.-H. *Inorg. Chem.* **2004**, *43*, 2759−2761.
(67) Mazurek, W.; Kennedy, B. J.; Murray, K. S.; O'Connor, M. J.; Rodgers, J. R.; Snow, M. R.; Wedd, A. G.; Zwack, P. *Inorg. Chem.* **1985**, *24*, 3258−3264.
(68) Nie, H.; Aubin, S. M. J.; Mashuta, M. S.; Porter, R. A.; Richardson, J. F.; Hendrickson, D. N.; Buchanan, R. M. *Inorg. Chem.* **1996**, *35*, 3325−3334.
(69) Krebs, B.; Zippel, F.; Ahlers, F.; Werner, R.; Haase, W.; Nolting, H. F. *Inorg. Chem.* **1996**, *35*, 3409−3419.
(70) Tuna, F.; Patron, L.; Journaux, Y.; Andruh, M.; Plass, W.; Trombe, J. C. *J. Chem. Soc., Dalton Trans.* **1999**, 539−545.
(71) Droege, M. W.; Satcher, J. H. Jr.; Weakley, T. J. R.; Taylor, R. T. *Inorg. Chem.* **1995**, *34*, 3317−3328.
(72) McKee, V.; Zvagulis, M.; Dagdigian, J. V.; Patch, M. G.; Reed, C. A. *J. Am. Chem. Soc.* **1984**, *106*, 4765−4772.
(73) Hay, P. J.; Thibeault, J. C.; Hoffmann, R. *J. Am. Chem. Soc.* **1975**, *97*, 4884−4899.
(74) Huang, S. F.; Chou, Y. C.; Misra, P.; Lee, C. J.; Mohanta, S.; Wei, H.-H. *Inorg. Chim. Acta* **2004**, *357*, 1627−1631.
(75) Sorell, T. N.; O'Connor, C.; Anderson, O. P.; Reibenspies, J. H. *J. Am. Chem. Soc.* **1985**, *107*, 4199−4206.
(76) Dirac, P. A. M. *The Principles of Quantum Mechanics*; Oxford University Press: Oxford, England, 1947.
(77) Soda, T.; Kitagawa, Y.; Onishi, T.; Takano, Y.; Shigeta, Y.; Nagao, H.; Yoshioka, Y.; Yamaguchi, K. *Chem. Phys. Lett.* **2000**, *319*, 223−230 and references therein.
(78) Hart, J. R.; Rappé, A. K.; Gorun, S. M.; Upton, T. H. *Inorg. Chem.* **1992**, *31*, 5254−5259.
(79) Sinnecker, S.; Neese, F.; Lubitz, W. *J. Biol. Inorg. Chem.* **2005**, *10*, 231−238.
(80) Ferreira, D. E. C.; De Almeida, W. B.; Neves, A.; Rocha, W. R. *Int. J. Quantum Chem.* **2009**, *110*, 1048−1055.
(81) Neese, F. *ORCA: An ab initio, density functional and semiempirical electronic structure package*, version 2.6, revision 04; Max Planck Institut fuer Physikalische und Theoretische Chemie: Berlin, Germany, 2007.
(82) Neese, F. *J. Phys. Chem. Solids* **2004**, *65*, 781−785.
(83) Neese, F. *Coord. Chem. Rev.* **2009**, *253*, 526−563.
(84) Berends, H. P.; Stephan, D. W. *Inorg. Chem.* **1987**, *26*, 754−759.
(85) Rompel, A.; Fischer, H.; Meiwes, D.; Büldt-Karentzpoulos, K.; Mangrini, A.; Eicken, C.; Gerdemann, C.; Krebs, B. *FEBS Lett.* **1999**, *445*, 103−110.
(86) Elgren, T. E.; Senior, S. Z.; Mans, L. L.; VanGuilder, H. D.; Kelly, K. A.; Hendrich, M. P. *Biochemistry* **2003**, *42*, 4392−4397.
(87) Krämer, R.; Kövári, E.; Heitker, J. *Chem. Commun.* **1995**, 1205−1206.
(88) Schenk, G.; Gahan, L. R.; Carrington, L. E.; Mitic, N.; Valizadeh, M.; Hamilton, S. E.; de Jersey, J.; Guddat, L. W. *Proc. Natl. Acad. Sci. U.S.A.* **2005**, *102*, 273.
(89) Deal, K. A.; Burstyn, J. N.; Hengge, A. C. *J. Am. Chem. Soc.* **1996**, *118*, 1713−1718.
(90) De Oliveira, M. C. B.; Couto, M. S. R.; Severino, P. C.; Foppa, T.; Martins, G. T. S.; Szpoganicz, B.; Peralta, R. A.; Neves, A.; Terenzi, H. *Polyhedron* **2005**, *24*, 495−499.
(91) Li, J.-H.; Wang, J.-T.; Hu, P.; Zhang, L.-Y.; Chen, Z.-N.; Mao, Z.-W.; Ji, L.-N. *Polyhedron* **2008**, *27*, 1898−1904.
(92) Rossi, L. M.; Neves, A.; Hörner, R.; Terenzi, H.; Szpoganicz, B.; Sugai, J. *Inorg. Chim. Acta* **2002**, *337*, 366−370.